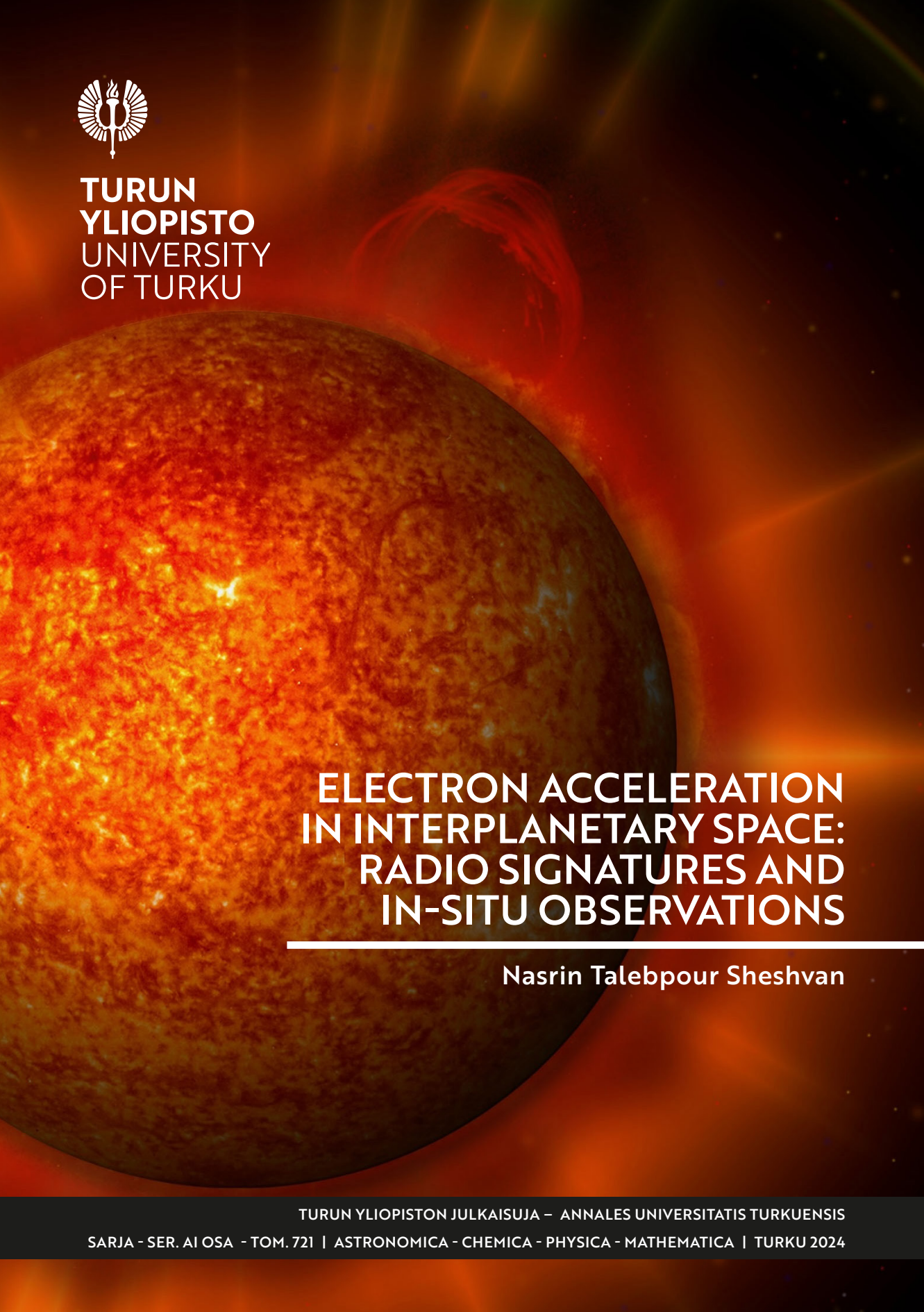

TURUN YLIOPISTO
UNIVERSITY OF TURKU

ELECTRON ACCELERATION IN INTERPLANETARY SPACE: RADIO SIGNATURES AND IN-SITU OBSERVATIONS

Nasrin Talebpour Sheshvan

TURUN YLIOPISTON JULKAISUJA – ANNALES UNIVERSITATIS TURKUENSIS
SARJA - SER. AI OSA - TOM. 721 | ASTRONOMICA - CHEMICA - PHYSICA - MATHEMATICA | TURKU 2024

UNIVERSITY OF TURKU

ELECTRON ACCELERATION IN INTERPLANETARY SPACE: RADIO SIGNATURES AND IN-SITU OBSERVATIONS

Nasrin Talebpour Sheshvan

TURUN YLIOPISTON JULKAISUJA – ANNALES UNIVERSITATIS TURKUENSIS
SARJA - SER. AI OSA - TOM. 721 | ASTRONOMMICA - CHEMICA - PHYSICA - MATHEMATICA | TURKU 2024

University of Turku

Faculty of Science
Department of Physics and Astronomy
Physics
Doctoral Programme in Exact Sciences

Supervised by

Dr. Silja Pohjolainen
University of Turku
Turku, Finland

Prof. Rami Vainio
University of Turku
Turku, Finland

Dr. Nina Dresing
University of Turku
Turku, Finland

Reviewed by

Dr. Miroslav Bàrta
Astronomical Institute of the Czech Academy of Sciences
Ondřejov, Czech Republic

Dr. Merja Tornikoski
Metsähovi Radio Observatory
Aalto University
Espoo, Finland

Opponent

Prof. Lidia van Driel-Gesztelyi
University College London
London, United Kingdom

Cover Image: Illustration of the twin STEREO spacecraft. Credit: NASA/ Jay Friedlander

ISBN 978-951-29-9798-5 (PRINT)
ISBN 978-951-29-9799-2 (PDF)
ISSN 0082-7002 (PRINT)
ISSN 2343-3175 (ONLINE)
Punamusta Oy, Turku, Finland, 2024

To my beloved parents, Esfandiar and Shahin

UNIVERSITY OF TURKU
Faculty of Science
Department of Physics and Astronomy
Physics
TALEBPOUR SHESHVAN, NASRIN: ELECTRON ACCELERATION IN INTERPLANETARY SPACE: RADIO SIGNATURES AND IN-SITU OBSERVATIONS
Doctoral dissertation, 138 pp.
Doctoral Programme in Exact Sciences
August 2024

ABSTRACT

Coronal Mass Ejections (CMEs) are large-scale releases of hot plasma, to which the magnetic field is frozen-in. If the CMEs are faster than the local magnetosonic velocity in the solar wind, they create shock waves as they travel through the corona and Interplanetary (IP) space. Shock waves driven by CMEs can accelerate Solar Energetic Particles (SEPs). Both phenomena involve the acceleration of electrons, which can be observed as electromagnetic radiation and plasma radiation.

This doctoral thesis presents analyses of the presence and propagation of accelerated electrons in the IP medium. By utilizing the observations of multiple science satellites, such as STEREO-A, STEREO-B, and Wind, we get a comprehensive picture of the accelerated particles and solar radio bursts, at various wavelengths. We can use this information to determine the origin of the eruptions, their directivity, and connections to other solar events. In particular, the role of shock waves in the acceleration of relativistic electrons is the subject of this research. Earlier studies have already confirmed the role of shock waves in the acceleration of electrons to keV energies using radio bursts, but for the higher energies, the research is still in progress.

As a result of observations by many space instruments we now have a 3D view of the Sun, particularly in the analysis of type IV radio bursts in multi-spacecraft radio dynamic spectra. The directivity of radio bursts, i.e., being seen only toward a certain direction, can be explained either by absorption in the surrounding medium or by obstruction of dense plasma region, even by the solar disk itself. The presence of dense plasma regions like solar streamers, in directions where no radiation is visible, strengthens this conclusion. Type II radio bursts can be associated with the interaction of streamers and shock waves. Our analysis of three separate type IV radio bursts revealed that their radiation was not visible toward directions where type II radio bursts were observed. The eruptions were generated by the same active region on three different days, and the location of the eruption region on the Sun changed from the disk center to the solar limb. The directivity of the type IV radio bursts could therefore be explained as absorption in the type II burst regions, as the shock fronts contain higher-density plasma.

In the study of isolated type II radio bursts, i.e., when separated from other bursts in time and also in frequency, we found that contrary to the previous studies, the majority of these radio bursts were associated with shocks that were created near the

CME leading fronts. The analysis suggests the necessity of special coronal conditions, to form this subgroup of low-frequency type II radio bursts.

The creation of relativistic electrons in IP shocks led to the investigation of whether these shocks can continue to accelerate electrons up to one Astronomical Unit (AU). Using in-situ observations of the electron flux, SEP events, and associated Energetic Storm Particle (ESP) occurrences, we identified nine cases observed by High Energy Telescope (HET) onboard STEREO where MeV electrons showed a significant increase associated with shocks driven by fast speed Interplanetary CMEs (ICMEs). We also found that such events were rare at a distance of 1 AU. The research suggests the necessity to make observations with satellites orbiting closer to the Sun, such as the Parker Solar Probe and Solar Orbiter, so that we can find out how electrons are accelerated in IP shocks. Finally, in-situ observations show clear signatures of local acceleration of electrons during the passage of the shock wave or the sheath region of the ICME during the ESP event.

KEYWORDS: Coronal mass ejection, shock wave, solar radio burst, long radio wavelengths, interplanetary space, high-energy particles

TURUN YLIOPISTO
Matemaattis-luonnontieteellinen tiedekunta
Fysiikan ja tähtitieteen laitos
fysiikka
TALEBPOUR SHESHVAN, NASRIN: ELECTRON ACCELERATION IN INTERPLANETARY SPACE: RADIO SIGNATURES AND IN-SITU OBSERVATIONS
Väitöskirja, 138 s.
Eksaktien tieteiden tohtoriohelma
elokuu 2024

TIIVISTELMÄ

Koronan massapurkauksissa (CME) Auringon koronasta vapautuu suuria määriä kuumaa plasmaa, johon magneettikenttä on kiinnittynyt. Jos massapurkaukset ovat nopeampia kuin paikallinen magnetosoninen nopeus aurinkotuulessa, ne aiheuttavat shokkiaaltoja matkatessaan koronan ja planeettainvälisen avaruuden halki. Massapurkausten synnyttämät shokkiaallot voivat kiihdyttää suurienergiaisia hiukkasia (SEP). Molempiin ilmiöihin liittyy elektronien kiihdytystä, joka voidaan havaita monen tyyppisenä sähkömagneettisena säteilynä, kuten plasmaemissiona.

Tässä väitöskirjassa esitetään analyysejä kiihdytettyjen elektronien olemassaolosta ja niiden etenemisestä lähiavaruuteen. Hyödyntämällä useiden eri tiedesatelliittien, kuten STEREO-A:n, STEREO-B:n ja Windin havaintoja saamme kattavan kuvan kiihdytetyistä hiukkasista ja Auringon radiopurkauksista useilla eri aallonpituuksilla. Voimme käyttää näitä tietoja määrittämään purkausten alkuperää, suuntaavuutta, ja yhteyksiä muihin Auringossa tapahtuviin ilmiöihin. Erityisesti shokkiaaltojen rooli relativististen elektronien kiihdytyksessä on tutkimuksen kohteena. Jo aikaisemmissa tutkimuksissa on radiopurkausten avulla vahvistettu shokkiaaltojen rooli elektronien kiihdytyksessä keV-luokan energioihin, mutta korkeampien energioiden osalta tutkimus on vielä kesken.

Monien eri satelliittien tallentamat radioaaltoalueen dynaamiset spektrit ja niissä havaitut tyypin IV radiopurkaukset mahdollistavat säteilylähteiden kolmiulotteisen paikantamisen Auringon lähiavaruudessa. Radiopurkausten suuntautuminen eli niiden näkyminen vain tiettyyn suuntaan voi selittyä joko väliaineessa tapahtuvan absorption tai tiheämmän plasma-alueen, jopa itse Auringon kiekon, peiton takia. Tiheäplasmaisten virtauslevyjen (streamer) esiintyminen sellaisissa suunnissa, joissa säteilyä ei näy, vahvistaa tätä johtopäätöstä.

Virtauslevyjen ja shokkiaaltojen kohtaamiseen tai törmäyksiin voi liittyä tyypin II radiopurkauksia. Tekemämme kolmen tyypin IV radiopurkauksen analyysi paljasti, että niissä säteily ei edennyt suuntiin, joissa havaittiin tyypin II radiopurkauksia. Purkaukset synnytti sama aktiivinen alue kolmena eri päivänä, jolloin purkausalueen paikka Auringon pinnalla siirtyi kiekon keskeltä lähelle kiekon reunaa. Tyypin IV radiopurkausten suuntaavuus voisi siten selittyä absorptiolla tyypin II purkausalueissa, koska shokkialtorintamissa on suurempi plasmatiheys.

Yksin, eli ajallisesti ja myös taajuusalueella muista purkauksista erillään esiin-

tyvien tyypin II radiopurkausten tutkimuksessa havaitsimme, että päinvastoin kuin aiemmissa tutkimuksissa, suurin osa radiopurkauksista syntyi sellaisten shokkiaaltojen yhteydessä, joissa shokkiaalto paikallistui CME:n etureunaan. Analyysi viittaa siihen, että tämäntyyppisen matalataajuisen tyypin II purkauksen syntyminen vaatii erityiset olosuhteet Auringon koronassa.

Relativististen elektronien syntyminen shokkiaaltorintamissa planeettainvälisessä avaruudessa johti tutkimaan, voivatko shokkiaallot jatkaa elektronien kiihdyttämistä jopa yhden AU:n etäisyydelle asti. Hyödyntämällä paikallisia havaintoja elektronivuosta, SEP-havaintoja ja niihin liittyvien suurienergiasten myrskyhiukkasten (ESP) esiintymistä, tunnistimme yhdeksän STEREO-satelliitin High Energy Telescope (HET) -instrumentin rekisteröimää tapausta, joissa MeV-luokan elektronit osoittivat merkittävää kasvua shokkiaalloissa, joihin liittyi nopeasti etenevä planeettainvälinen CME (ICME). Havaitsimme myös, että tällaiset tapahtumat olivat harvinaisia yhden AU:n etäisyydellä. Tutkimus viittaa tarpeeseen tehdä havaintoja lähempänä Aurinkoa esimerkiksi Parker Solar Probe - ja Solar Orbiter -tutkimussatelliiteilla, jotta voimme selvittää, miten elektronit kiihtyvät shokkiaaltorintamissa planeettainvälisessä avaruudessa. In situ -havainnoissa voimme lisäksi nähdä selviä merkkejä elektronien paikallisesta kiihdytyksestä shokkiallon tai ICME:n turbulentin välivyöhykkeen (sheath) ohituksessa ESP-tapahtumien aikana.

AVAINSANAT: Koronan massapurkaus, shokkiaalto, Auringon radiopurkaus, pitkät radioaallonpituudet, planeettainvälinen avaruus, suurienergiaiset hiukkaset

Acknowledgements

Thinking back to getting my Master's degree, I can finally pause and appreciate how far I've come. Although I started a PhD program in high-energy astrophysics at Middle East Technical University, my love for our star, the Sun, never dimmed. That passion led me to the Tuorla Observatory in 2015, where I first saw the aurora borealis - a celestial ballet of vibrant colors and vast expanse.

My heartfelt gratitude goes to Dr. Silja Pohjolainen, my first supervisor, who graciously responded to an email from a young space physics enthusiast. Thank you, Silja, for your continued support during my challenging times, for introducing me to the fascinating field of radio bursts, and for your invaluable guidance throughout my PhD journey.

Special thanks go to my second supervisor, Prof. Rami Vainio. I am truly grateful for your unfailing support and constant encouragement. Your brilliant ideas and insightful comments were crucial in shaping this research. Thank you for believing in my potential and the opportunities you provided me to collaborate on exciting national and international projects.

The completion of this thesis owes much to the contributions of my third supervisor, Dr. Nina Dresing. I am grateful for your willingness to share your broad knowledge of electrons, your patience, and always being available to answer my numerous questions. I learned so much from you and truly enjoyed your company during the final stage of this research.

I am truly honored that Prof. Lidia van Driel-Gesztelyi has agreed to travel to Finland and be my opponent for the thesis defense. I would also like to express my gratitude to the pre-examiners, Dr. Miroslav Bàrta and Dr. Merja Tornikoski, for their careful review of my thesis and insightful comments.

A big thank you to the current and past members of the Space Research Laboratory for creating such a welcoming and positive work environment. To my wonderful friends, who have made these years enjoyable and awesome, I feel so lucky to have such dependable and encouraging people around me.

My deepest gratitude extends to the solid foundation on which I stand, my family. To my beloved parents Shahin and Esfandiar, my brother Bijan and his family, and my sister Narmin, I offer my most heartfelt thanks for your unconditional love and continuous support. Through the years, you have been a constant source of joy, strength, and belief in my abilities.

To Melina, the cherished and lovely memories we have built together are evidence of the depth of our connection. Your presence has enriched my life in countless ways. You are, in essence, my chosen family. I eagerly look forward to all the beautiful experiences and discoveries to come.

Finally, to Armin, I express my most heartfelt gratitude. For all these years, you have showered me with love, support, encouragement, and faith. We've already filled so many pages in our life's adventure together. Here's to keeping the story exciting with many more chapters to come!

Turku, June 2024
Nasrin Talebpour Sheshvan

Table of Contents

Abbreviations

AIA	Atmospheric Imaging Assembly
AU	Astronomical Unit
CIR	Co-rotating Interaction Region
CME	Coronal Mass Ejection
DH	Decameter–Hectometer
ESP	Energetic Storm Particle
EUV	Extreme UltraViolet
EVE	Extreme Ultraviolet Variability Experiment
GBSRBS	Green Bank Solar Radio Burst Spectrometer
GOES	Geostationary Operational Environmental Satellite
HET	High Energy Telescope
HMI	Helioseismic and Magnetic Imager
ICME	Interplanetary CME
IMPACT	In situ Measurements of PArticles and CME Transients
IP	Interplanetary
LASCO	Large Angle Spectroscopic Coronagraph
LET	Low Energy Telescope
MAG	Magnetic Field Experiment
MHD	Magnetohydrodynamic
NDA	Nançay Decameter Array
PFSS	Potential Field Source Surface
PLASTIC	PLAsma and SupraThermal Ion Composition
RSTN	Radio Solar Telescope Network
SDO	Solar Dynamics Observatory

SECCHI	Sun–Earth Connection Coronal and Heliospheric Investigation
SEP	Solar Energetic Particle
SEPT	Solar Electron and Proton Telescope
SIR	Stream Interaction Region
SIT	Suprathermal Ion Telescope
SOHO	Solar and Heliospheric Observatory
SRBS	Solar Radio Burst Spectrometer
STE	Suprathermal Electron Instrument
STEREO	Solar TErrestrial RElations Observatory
SWEA	Solar Wind Electron Analyzer
XRS	X-ray Sensor

List of Symbols

K	Kelvin: Thermodynamic temperature
J	Joule: Energy
eV	Electron-volt: Energy
UT	Universal Time
Å	Angstrom
$R_\odot$	Solar radius
V_{ms}	Magnetosonic speed
V_A	Alfvén speed
V_s	Sound speed
B	Magnetic field magnitude
μ_0	Permeability of vacuum
ρ_m	Mass density of plasma
γ	Adiabatic index
k_B	Boltzmann constant
T	Temperature
m	Mean mass
f	Frequency
Hz	Hertz: Frequency
n_e	Electron density
n_0	Electron density near Earth
R_d	Distance from the Sun

υ	Shock velocity
H	Density scale height
L1	Lagrangian equilibrium point
M_A	Alfvénic Mach number

List of Original Publications

This dissertation is based on the following original publications, which are referred to in the text by their Roman numerals:

I N. Talebpour Sheshvan, S. Pohjolainen.
Visibility and Origin of Compact Interplanetary Radio Type IV Bursts.
Solar Physics, 2018; 293, 148.

II S. Pohjolainen, N. Talebpour Sheshvan.
Cut-off features in interplanetary solar radio type IV emission.
Advances in Space Research, 2020; P. 1663-1672, 65, 6.

III S. Pohjolainen, N. Talebpour Sheshvan.
Formation of Isolated Radio Type II Bursts at Low Frequencies.
Solar Physics, 2021; 296, 81.

IV N. Talebpour Sheshvan, N. Dresing, R. Vainio, A. Afanasiev, D. E. Morosan.
On the role of interplanetary shocks in accelerating MeV electrons.
Astronomy & Astrophysics, 2023; 674: A133.

List of Publications not included in the thesis

V Afanasiev, A., Vainio, R., Trotta, D., Nyberg, S., Talebpour Sheshvan, N., Hietala, H., Dresing, N.
Self-consistent modeling of the energetic storm particle event of November 10, 2012.
Astronomy & Astrophysics, 2023; 679: A111.

VI Pohjolainen, S., McKay, D., Talebpour Sheshvan, N. Monstein, C.
Repeated Type III Burst Groups Associated with a B-Class Flare and a Narrow-Width CME.
Solar Physics, 2023; 298: 118.

VII Pohjolainen, S., Talebpour Sheshvan, N. Monstein, C.
Separating the effects of earthside and far side solar events. A case study.
Advances in Space Research, 2023; P. 4074-4081, 72, 9.

1 Introduction

The term *Space weather* refers to the time-varying conditions in the heliosphere, which directly depend on solar magnetic activity (Palmerio et al. 2018). Therefore, the origin and the structure of the Sun's magnetic field need to be studied to understand how it governs various solar activities and how it propagates and behaves in space.

The Sun is a medium-sized star composed of two major parts, the interior and the atmosphere. The interior part is the combination of three layers: the core, the radiation zone, and the convection zone. The energy produced through nuclear reactions gradually moves outward by radiative diffusion in the hot core. Beyond the radiative zone, the transfer occurs through convection, allowing the hot plasma to move in a cycle from the bottom to the surface, cooling down and descending back down to the bottom. This motion contributes to the generation of the magnetic field of the Sun.

After passing through the convection zone, the energy reaches the solar atmosphere, separated into the photosphere, chromosphere, transition region, and corona. The photosphere is a relatively thin layer with a temperature of around 5800 K. It is the Sun's visible surface and shows one of the important activities of the Sun by dark sunspots. The chromosphere is located above the photosphere, with a temperature between $4 - 8 \times 10^3$ K that changes with height. A very thin layer above the chromosphere is called the transition region with a temperature increasing and reaching 500×10^3 K. Corona is the Sun's outermost atmospheric layer, which extends far into space, consists of hot plasma (up to a few million kelvins) and is visible during total solar eclipses and coronagraph imaging (Section 3).

The Sun is an active star that exhibits signatures of its activity across the entire electromagnetic spectrum. It is a ball of hot plasma and – in addition to radiating energy from radio waves to gamma rays – it shapes the heliosphere by continuously releasing plasma to IP space. These continuous outflows are called the solar wind (e.g., Coles & Maagoe 1972; Echim et al. 2011). Observing the Sun at different wavelengths (Fig. 1) provides a comprehensive and valuable understanding of the different components of solar activity and variability. In addition, it improves our understanding of how particles are accelerated in solar phenomena and how they propagate through the heliosphere. Solar eruptions are the common indicators of solar activity resulting from disruptions or transitions within the solar wind. They are leading drivers of the acceleration of electrons and the various space weather

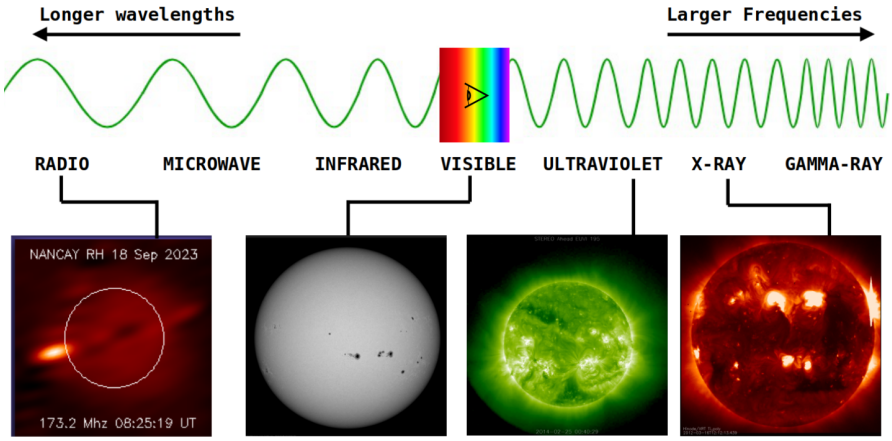

Figure 1. Four images of the Sun taken in radio (NRH at 173 MHz), optical (SDO/HMI at 450 nm), Extreme-ultraviolet (STEREO/EUVI at 195 Å), and X-ray (Hinode/XRT) wavelengths.

phenomena and can originate and occur across diverse temporal and spatial scales.

Radio bursts are signatures of solar activity and a reference to study the flaring and eruptive processes, generally, in the Sun-type stars (Crosley & Osten 2018). They act as early indicators of the onset and initial development of CMEs before becoming visible in coronagraphs or the presence of shock waves in the corona and shed light on the necessary condition for energetic particles to escape from the corona (Klein 2021a). The signatures of radio emissions and their evolution in the dynamic spectrum are key to understanding the relationship between the Sun and the heliosphere. Analysis of radio spectral data, in the absence of radio imaging at low frequencies, is a tool to connect ground-based observations with space observations, to observe the Sun and its disturbances of the plasma continuously, and to serve space weather monitoring and forecasting purposes.

The overall goal of this research is to improve our understanding of the central open questions in solar physics: How do solar eruptions and the resulting shock waves energize and transport particles in the corona and IP medium, and how can we observe these processes using radio emissions and energetic particles detected by spacecraft? The combined research work of this thesis aims to gain a more comprehensive picture of how solar eruptions accelerate and transport particles, interpret radio emissions produced by accelerated electrons, and finally, contribute to a more detailed analysis of solar activity and its potential effects on space weather.

In particular, this thesis addresses the following major issues:

- How do the location, source characteristics, and propagation environment in-

fluence the properties of solar radio bursts, particularly type IV bursts? (Paper I and Paper II)

- How do solar eruptions and coronal conditions influence the formation of different radio emissions, and how do dense plasma structures in the IP medium affect the visibility and propagation of radio bursts? (Paper I and Paper III)
- How do solar eruptions and their associated phenomena accelerate energetic electrons in the interplanetary medium? (Paper IV)

This dissertation presents the observational analysis of selected radio bursts that propagated into the IP space. Chapter 2 presents an introduction to solar eruptive phenomena and their role in accelerating and propagating particles into the inner heliosphere. In chapter 3 different space and ground-based observatories and their provided data are introduced. In the same chapter, the methods of temporal and spectral analysis used in defining emission mechanisms, and the conditions in shocks for electron acceleration to relativistic energies, are also discussed. Chapter 4 summarizes the original publications included in this dissertation.

2 Signatures of the active Sun

2.1 Solar flares

Solar flares are known as dynamic events characterized by the sudden release of huge energy ($\geq 10^{25}$ J) via magnetic reconnection, in time scales from a few to tens of minutes (Chen et al. 2020; Jiang et al. 2021; Yan et al. 2022). The sudden energy release process can be observed as a rapid brightening of reconnecting magnetic fields in the corona, and it covers a wide range of wavelengths from decameter radio waves to gamma rays over 1 GeV (e.g., Benz 2017, and references therein).

The first observation of a solar flare was in 1859, known as the Carrington event (Carrington 1859; Hodgson 1859). The *white-light flare* was estimated to have been equivalent to an X-ray flare of ~ X45 class (Cliver & Dietrich 2013, see the GOES classification in section 3.1.5). In comparison, the most powerful flare in our times was estimated to have the ~ X28 class (Thomson et al. 2004). Many studies have confirmed that a portion of this energy heats the local plasma, and most of the energy is used to accelerate particles along open or closed magnetic field lines (Reames 1990; Mann et al. 2006; Cheng et al. 2018).

Accelerated particles play an important role in the production of electromagnetic radiation from solar flares. The big picture of the flare time-intensity profile at several wavelengths helps to improve the knowledge of the different emissions in the same flare. The first phase is the time when the coronal plasma is gradually heated in the flare region. It can be observed in soft X-ray and Extreme UltraViolet (EUV), and is known as the *preflare phase*. The next period is called the *impulsive phase* when a large portion of the energy is released and a large number of energetic electrons and ions are accelerated. As a robust evidence for this phase is the existence of hard X-ray sources (Hoyng et al. 1981). A fraction of trapped energetic particles also cause intensive emissions in the radio bands in this phase.

Then, during the flare *decay phase* the surrounding plasma reverts back to its initial state. However, in the magnetic reconfiguration distance ($> 1.2\ R_\odot$), high-speed CMEs continue to accelerate particles, when they are associated with shock waves. This activity leads to meter-wave radio bursts that can continue to decameter-hectometer (DH) wavelengths and IP particle events (more information is available in the Benz (2017) and references therein).

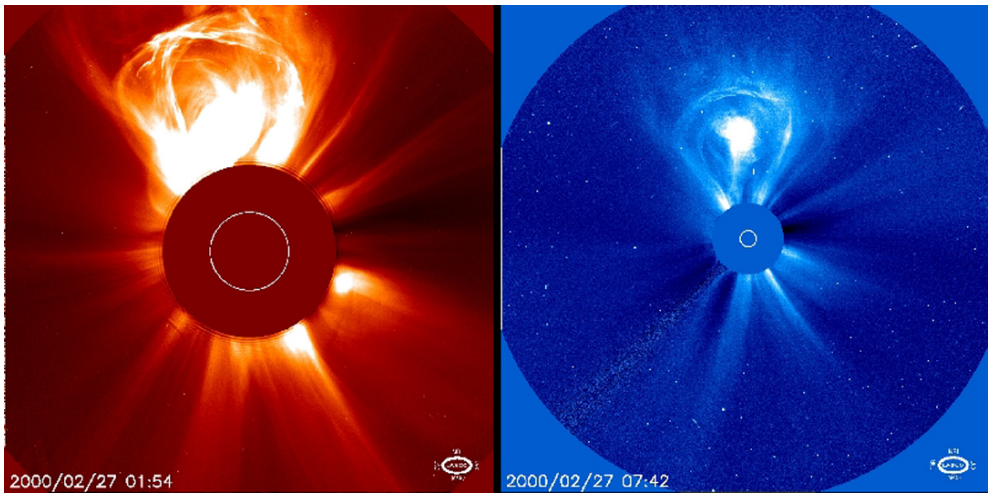

Figure 2. Coronagraph images of a CME on 27 February 2000, observed by SOHO LASCO C2 (Left panel) and C3 (Right panel). Image credit: ESA–NASA SOHO/LASCO.

2.2 Coronal mass ejections

CMEs (Webb & Howard 2012) are another spectacular eruption of plasma and magnetic field. They propagate from the solar atmosphere to large spatial distances in the heliosphere. These extreme explosions can eject $\sim 10^{12} - 10^{16}$ kg of magnetized plasma with kinetic energies exceeding $\sim 10^{25}$ J and speeds ~100 – 3000 km s^{-1} (Howard et al. 1985; Yashiro et al. 2004; Yurchyshyn et al. 2005; Gopalswamy et al. 2010; Vourlidas et al. 2010; Webb & Howard 2012). The discovery of CMEs dates back in the early seventies (Tousey 1973; MacQueen et al. 1974, named as coronal transients) when they were observed by coronagraphs as Thomson scattered white light from the electrons in the transient cloud of plasma. White light images of CMEs, observed by the Large Angle Spectroscopic Coronagraph (LASCO) C3 and C2 coronagraphs on board the Solar and Heliospheric Observatory (SOHO) are presented in Fig. 2.

CME mass may include filament material, as CMEs are often accompanied by eruptive prominences. The classic parts of the CME include the bright compression edge known as *front*, while the sides are called *flanks*. The *core* of a CME is a bright and dense structure formed by the ejected solar material and prominence close to the Sun's surface, while the *cavity* is a darker region that surrounds the core and is characterized by a lower material density compared to the core. Halo CMEs appear all around the solar disk, like a halo, and they can be directed towards the Earth or the opposite direction when the source origin is on the backside of the Sun. Halo-CMEs were first detected by *Solwind* (Howard et al. 1982).

One classification divides CMEs into impulsive and gradual types, based on the

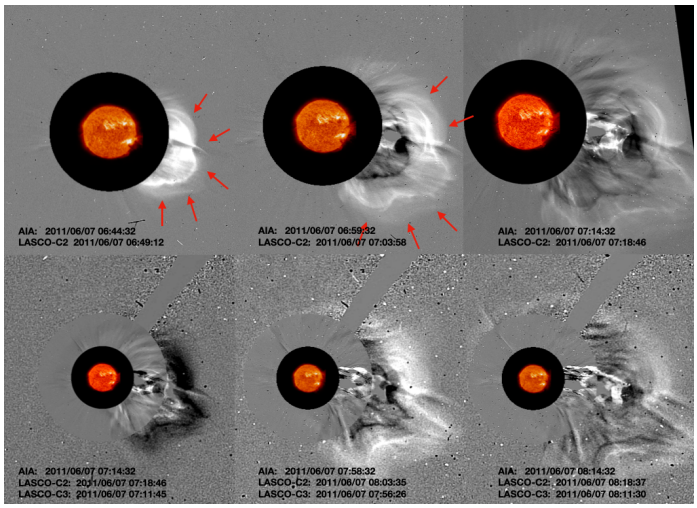

Figure 3. The sequence of running-difference images obtained with LASCO-C2 and LASCO-C3, with SDO/AIA 304 Å in the middle, shows the propagation of a CME-driven shock. The red arrows denote the faint shock front in the first two images (images created with JHelioviewer).

duration and speed range. Another classification refers to the apparent shape of the CMEs in white-light images. More recent studies accept a complex CME structure, that includes several magnetic flux systems and neutral lines. Since the 20th century, phenomena associated with CMEs such as flares and prominences have been documented. After that, energetic particles, type II and type IV radio bursts, and IP shocks have been detected (e.g., Forbush 1946; Wild et al. 1954; Sonett et al. 1964). When CMEs propagate into the heliosphere, they disturb the coronal surroundings and create density enhancements, that lead to changes in observable structures. The time of observable structures varies between several minutes to several hours (Schwenn 2006). The CMEs that maintain their shapes and structures in longer distances become ICMEs and can reach and pass even the orbit of the Earth (Vilmer et al. 2003; Jian et al. 2006).

2.3 Shocks

In addition to CMEs, solar flares are able to generate turbulence and drive shocks in the lower parts of the corona (e.g., Hundhausen 1989). CMEs are observed using the white-light coronagraph and often appear as bright loops with a fainter emission surrounding them. This faint emission marks a shock front (Fig. 3). A shock wave (e.g., Parks 2004; Koskinen 2011) can be formed when a CME moves through the

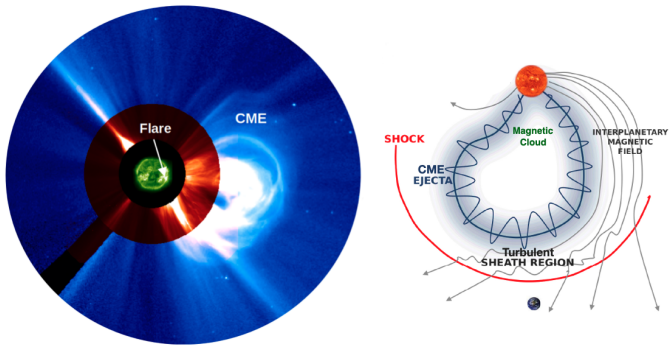

(a) The combination of SOHO/LASCO C2 and C3 images of a CME produced by JHelioviewer (Müller et al. 2017) with the flare location shown with the white arrow on the SOHO/EIT image (left). Schematic drawing of the ICME associated with the shock represented with red arc (right), adapted from Kilpua et al. (2017).

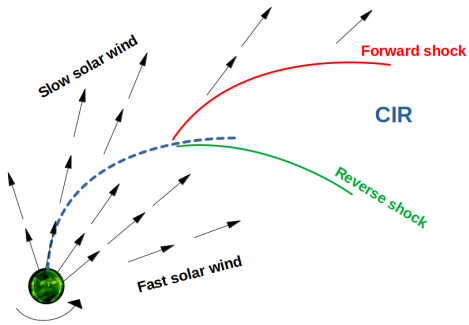

(b) Forward and reverse shock pair related to CIR

Figure 4. Two types of interplanetary shocks

plasma faster than the local magnetosonic speed, V_{ms} (Vourlidas et al. 2003, 2013),

$$V_{ms} = \sqrt{V_A^2 + V_S^2}.$$

The magnetosonic speed is a combination of the *Alfvén speed* $V_A = \sqrt{B^2/\mu_0\rho_m}$, and the *sound speed* of a fluid $V_S = \sqrt{\gamma k_B T/m}$. Here, B is the ambient magnetic field magnitude, μ_0 is the permeability of vacuum, ρ_m is the mass density of plasma, γ is the adiabatic index, k_B is the Boltzmann constant, T is the temperature, and m is the mean mass of the plasma particles. When the supersonic solar wind encounters magnetized planets, it generates bow shocks in front of them (Tidman 1967). The most detailed analyses in the topic of planetary bow shocks is the development of the bow

shock in front of Earth, due to the interaction of incoming solar wind with Earth's magnetosphere. Additionally, the IP counterpart of a CME is capable of driving various IP shock waves from the Sun to large heliospheric distances (Richardson et al. 2006). Fast ICMEs are capable of driving a bow shock ahead of them, as illustrated in Fig. 4a. As Oh et al. (2007) highlighted, these shocks represent the most common types observed at 1 AU during solar maximum.

In addition to the shocks formed by supersonic CMEs, there exists yet a second group formed by the interaction of the fast and slow solar wind. As the Sun rotates, the fast solar wind catches up with the slower and denser ambient solar wind, creating an interaction region known as a Stream Interaction Region (SIR). This interaction region can be delineated by forward and reverse propagating waves. However, at larger distances, the SIRs strengthen and become capable of generating a pair of forward and reverse shock waves on either side of the Co-rotating Interaction Region (CIR) (Fig. 4b Hundhausen 1972; Hundhausen & Gosling 1976).

Previous studies show a consensus that CMEs are the main driver for the IP shocks (Gopalswamy 2006). But two possible and acceptable hypotheses of the origin of shock waves are related to both CMEs and flares or their combination (Shanmugaraju et al. 2005; Cho et al. 2005; Pohjolainen & Lehtinen 2006; Gopalswamy 2006). The physical interpretation is that the driver of the shock waves over large distances could be a CME, or could be related to the process of energy release on a smaller scale by flare in a distinct way, e.g., through the development of hot loops or small-scale ejections (Klassen et al. 2003; Dauphin et al. 2006). The well-known signatures of propagating shock waves in the corona (e.g., Mancuso et al. 2019; Morosan et al. 2020) are radio type II bursts (Nelson & Melrose 1985; Mann et al. 1996; Kumari et al. 2017; Vršnak & Cliver 2008; Nindos et al. 2008).

2.4 Coronal streamers

Coronal streamers are elongated, large-scale structures that can be detected in the white-light coronograph images. They sometimes confine the expanding CME structures, and stay unaffected by them (Bemporad et al. 2005). The streamers are brighter than the surrounding medium because of higher plasma density with low Alfvén speed (Habbal et al. 1997; Strachan et al. 2002; Kwon et al. 2013). However, sometimes the streamers could be subjected to a forceful ejection and are torn apart (Vourlidas & Webb 2018). They have the physical appearance of an open magnetic field rooted to the surface of the Sun, extending to several solar radii (McLean & Labrum 1985; Aschwanden 2004).

Continuous interaction of the streamers with different solar eruptions like CME (e.g., Chen et al. 2011; Chen 2013), prepare the conditions for accelerating the electrons and causing further events. For example, transport of electron beams from the solar surface to the IP space leads to metric and decameter–hectometer (DH) radio

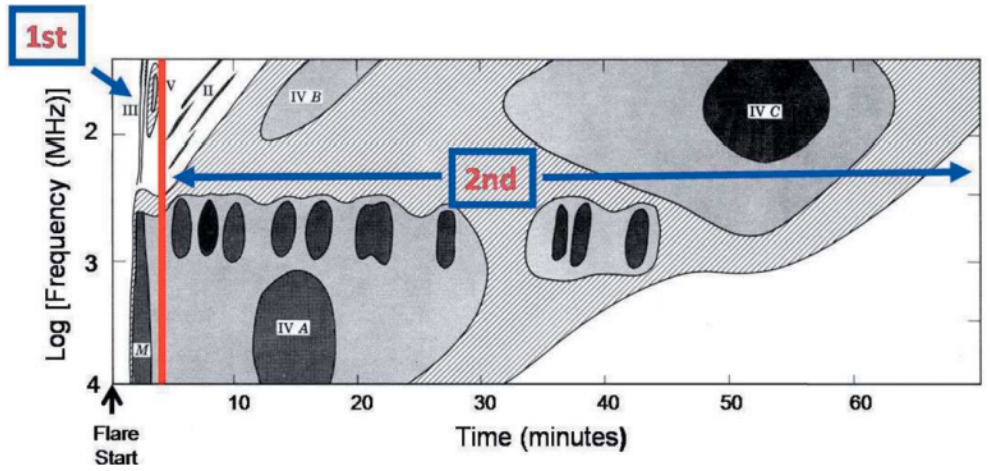

Figure 5. A schematic dynamic spectrum of the two phases of developed radio burst. The red vertical line separates the impulsive phase and the shock-associated phase. In most cases, the first phase of radio bursts occurs during flares. (Wild et al. 1963). The figure is adopted from Cliver (2009)

emissions (e.g., Kong et al. 2012; Shen et al. 2013; Chen et al. 2014).

2.5 Solar energetic particles

SEP events are generally associated with solar eruptions like flares and CMEs, and they are composed of electrons, protons, and heavier ions. These are transient injections, with a broad range of energy from keVs up to GeVs. The birth of research in the field of SEP physics started with indicating significant increases in the intensity of cosmic ray particles with energies around 1 GeV (referred to as ground-level events), observed in 1942 (Forbush 1946).

The first theory of SEP events was introduced by Meyer et al. (1956). They suggested that the short duration of SEP events was caused by solar flares and that scattering in IP space was responsible for the longer duration particle events. The more comprehensive theory presented by Wild et al. (1963) determined two phases in the SEP acceleration processes in flares (Fig. 5). First, primarily accelerated electrons ($\sim$ 100 keV) are observed as fast drift type III radio burst emission. Slow drift type II radio emission at metric wavelengths revealed the second phase of a large flare, produced by a propagating magnetohydrodynamic shock with speed $\sim$ 1000 km s^{-1}.

The accelerated particles in IP space and near-Earth space are classified into two categories of impulsive and gradual SEP events. Impulsive SEP events, characterized by lasting hours, are notable for their electron-rich composition. The processes of

impulsive SEP acceleration include wave-particle interactions and reconnection associated with flares and jets. These events are limited to the region in the vicinity of the magnetic field lines directly linked to the active region. Gradual SEP events, on the other hand, are more intense and electron-poor (proton-rich) events, they last for days and are associated with coronal shock waves, driven by CMEs that accelerate energetic charged particles into IP space (e.g., Shea & Smart 1990; Reames 2004, 2017; Desai & Giacalone 2016). Due to the broad IP shock, gradual SEP events exhibit wide longitudinal distributions. The temporal profile of the particle intensity is affected by the dynamic changes in shock strength and the observer's location in relation to the traveling shock (Heras et al. 1995; Aran et al. 2018).

Local enhancements of charged particles at the time of IP shock passing the spacecraft are referred to as ESP events (Gosling et al. 1981; Tsurutani & Lin 1985). Most of the time, the ESP events occur at the shock following the early accelerated SEPs in the IP medium (Fig. 6). However, in some unique cases, ESP can occur as isolated events, without a previous SEP event (Paper IV).

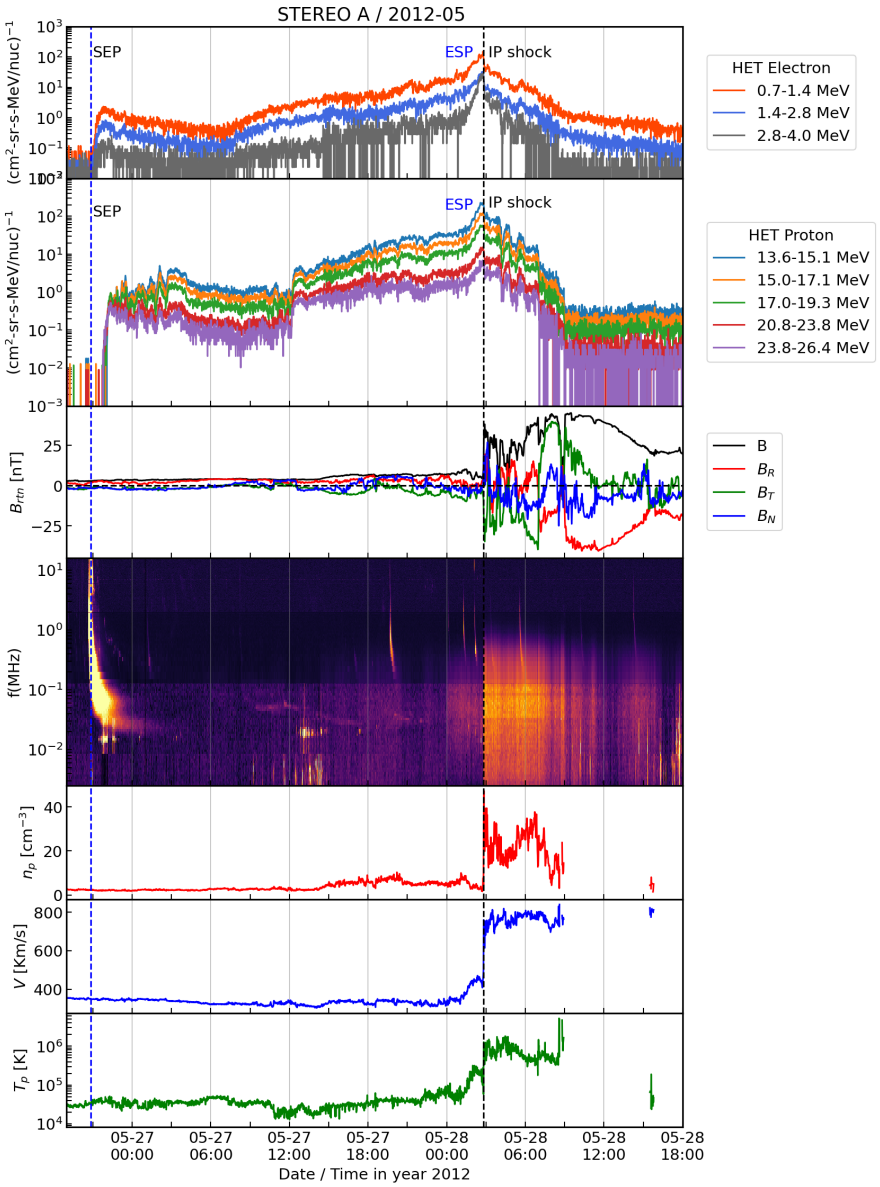

Figure 6. SEP event on 27 May 2012 and a corresponding ESP event on 28 May 2012. The blue vertical dashed line marks the onset time of SEPs and the black marks the time of shock arrival at the STEREO-A on 28 May 2012. From top to bottom, the electron and proton time-intensity profiles measured by the HET instrument, the magnetic field changes, and its components in RTN coordinates measured by the in-situ measurement (IMPACT/MAG), STEREO/WAVES dynamic spectrum. The following three panels present measurements from PLASTIC, including plasma density, bulk solar wind speed, and temperature.

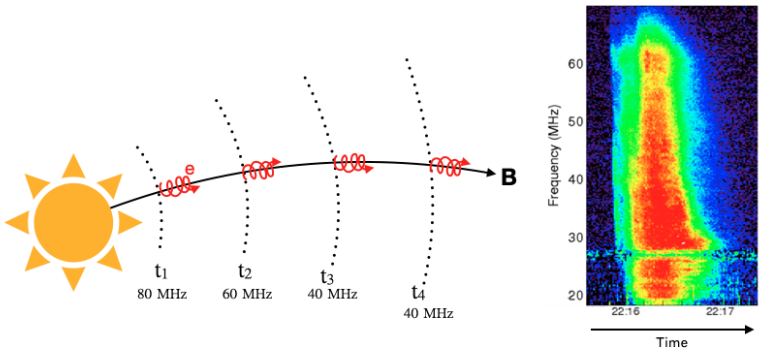

Figure 7. Schematic diagram of a radio source moving away along an open magnetic field line (dynamic spectra of the type III radio burst recorded by GBSRBS). The t_1 to t_4 represent the time period when the source drifts from higher to lower frequencies. The figure is reproduced from Chrysaphi (2021).

2.6 Radio bursts

The starting point of solar radio astronomy goes back to World War II. Unknown radio emission was detected when the aerial medium was monitored for aircraft detection (McLean & Labrum 1985). It was the detection of these emissions that opened up a new field of study for physicists and radio engineers, giving them the motivation to develop instruments for scientific studies. The preliminary studies found a correlation between the observed events and the active regions on the Sun (Appleton & Hey 1946). The term *radio bursts* has been mentioned by the study of Payne-Scott et al. (1947) to record and investigate the intensities of solar emissions. Dynamic spectrum is a diagram showing the intensity of the emissions as a function of frequency versus time. The appearance of emissions with higher frequency is caused by radio sources located close to the Sun. With increasing distance of a radio source from the Sun, the emission frequency decreases over time (Fig. 7, see, e.g., Section 3.2.1).

Radio bursts and energetic particles have been linked since their discovery in 1942 and their association with non-thermal particles during solar activity phenomena has been established. Investigation of radio burst signatures enhances our understanding of the acceleration and propagation of energetic particles in the corona and the IP medium (e.g, Vourlidas et al. 2020; Reid 2020). Wild & McCready (1950) recognized three different types of features in radio bursts that appeared in the dynamic spectra. They were classified as type I, type II, and type III bursts. Type IV and type V radio bursts (Wild et al. 1959b, 1963) were identified shortly after, see, for example, Aschwanden (2005). Fig. 8 shows how radio bursts appear and propagate in the

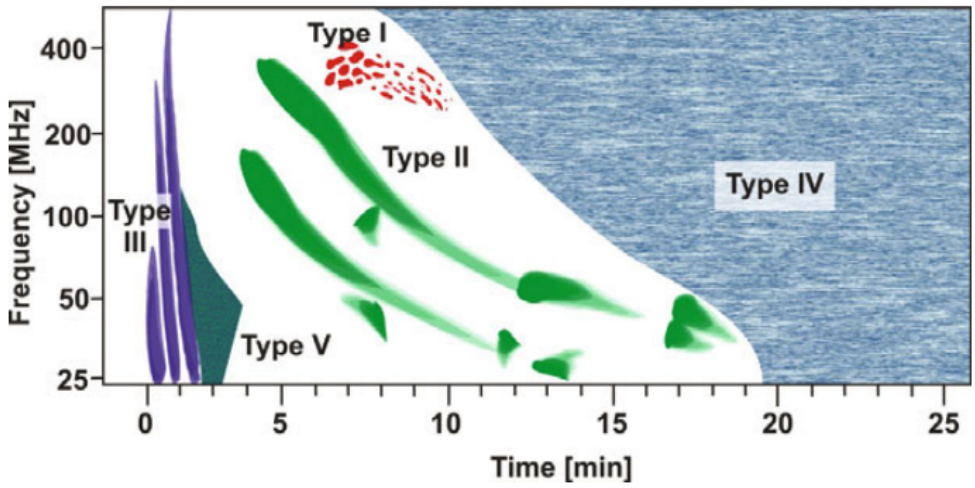

Figure 8. Visual diagram of the different forms of the classical categories of the type I to type V radio bursts as observed through dynamic spectra. Reproduced from Dąbrowski et al. (2016).

dynamic spectrum. Characterization of radio bursts, like frequency-drift ($\frac{df}{dt}$), duration (Δt) and total bandwidth (Δf) of the emission can provide valuable information about the solar source and also the local coronal conditions (see Fig. 9).

Radio bursts with fine structures can be narrow-band and short-lived emissions that appear alone, or they can be observed within a broader emission structure on the dynamic spectrum (Chernov et al. 2007, 2014; Armatas et al. 2019). They are detectable when high-time resolution spectra are available. Their investigation can give insight into the conditions and mechanisms that caused such radio emissions.

2.6.1 Type I radio burst

The most common phenomenon at metric wavelengths, with a very short duration is known as a type I solar radio burst (Elgarøy 1977). In dynamic spectra, they appear as spike-like, in chains, and with narrow bandwidths. When they appear in a group looking like a continuum emission (long duration and wide bandwidths), this is called a noise storm. Both the bursts and the noise storm can be highly polarized (Mugundhan et al. 2018; McCauley et al. 2019) and can occur at the same time. These phenomena originate from trapped, non-thermal electrons associated with emerging magnetic fields (Benz & Wentzel 1981; Spicer et al. 1982).

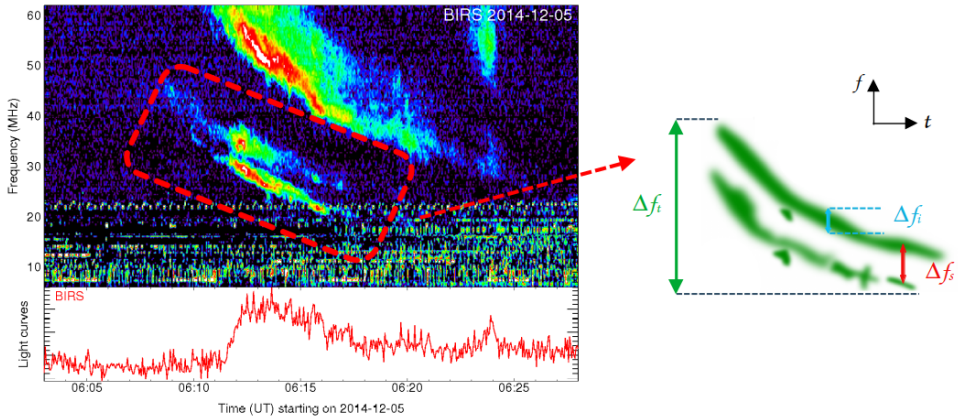

Figure 9. Dynamic spectra from BIRS, indicating type II radio emission with fundamental and harmonic lanes, both have experienced band-splitting. Schematic illustration of the different bandwidths presented in a type II radio burst: Δf_t (green) is the total bandwidth of the emission, Δf_i (blue) is the bandwidth of the emission lane in real-time, and Δf_s (red) is the frequency split between the two lanes. The two-banded emission of type II radio burst is adopted from Ganse et al. (2012).

2.6.2 Type II radio burst

Type II radio bursts appear in dynamic spectra as slowly drifting features, from high to low frequencies (McLean & Labrum 1985). Two examples of type II radio bursts are demonstrated in Fig. 9 and Fig. 10. It has been confirmed that type II radio bursts are closely associated with the acceleration of energetic electrons at shock waves. They can be triggered by CMEs, flares, and erupting filaments (see, e.g., Nindos et al. 2011; Magdalenić et al. 2012; Grechnev et al. 2016, 2018; Kumar et al. 2016; Jebaraj et al. 2020).

The frequency range for the appearance of type II radio bursts in dynamic spectra is separated into three groups. First, the metric range includes frequencies from 300 MHz to 30 MHz, then the decametric range extends from 30 to 3 MHz, and last is the hectometric range that covers 3 MHz to 300 kHz. The first detection of IP type II bursts, below the Earth's ionospheric cut-off frequencies that happen near 25 MHz, was in spacecraft data (Cane et al. 1982). The acceleration mechanism of electrons in solar eruptions is still one of the unsolved issues of solar physics, but in type II radio bursts they are locally accelerated at the traveling shock. Therefore, IP type II radio bursts are linked to CMEs and propagating shock waves, with non-linear Langmuir-wave processes that create plasma emission at the fundamental and harmonic plasma frequencies (Cane & Stone 1984; Lengyel-Frey 1992; Reiner et al. 1998; Robinson

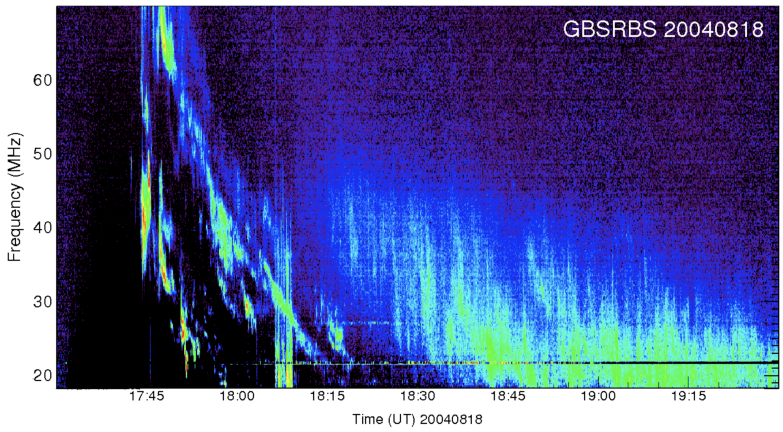

Figure 10. Dynamic spectra of classic radio bursts of type II and type IV on 18 August 2004, recorded by GBSRBS at 70–20 MHz.

& Cairns 2000).

2.6.3 Type III radio burst

The most common and intense radio emissions that last for a few seconds (Wild & McCready 1950; McLean & Labrum 1985) are type III radio bursts, easily determined with a sharp appearance on the dynamic spectra, with a broad starting frequency range, and fast drift from high to low frequencies ($\sim$100 MHz s^{-1}). Based on the strength of origin, type III radio bursts have been observed at a wide frequency range between 1 GHz and 10 kHz.

According to van Allen & Krimigis (1965), who investigated the first observations of energetic particles, energetic electron events have a close relation to type III radio emissions. Both observations and theory support this statement (e.g., Gosling et al. 2003; Krucker et al. 2007; Wang et al. 2012). A Type III radio burst is generated by energetic electron beams that are accelerated during flares and travel along open magnetic field lines in the corona (e.g., Reid & Ratcliffe 2014). Therefore, they are valuable tools for studying electron acceleration and magnetic field properties during solar eruptions.

2.6.4 Type IV radio burst

Type IV radio bursts are described as broadband continuum emissions that appear in the metric to decimetric (Benz 1980) wavelengths in the dynamic spectrum. The

radio continua in metric ranges are categorized into the moving and stationary type IV (Weiss 1963; Melrose 1980). The burst duration varies from tens of minutes to a few hours (McLean & Labrum 1985). The stationary bursts originate from the magnetic structure over the active regions or post-eruption arcades associated with CMEs (Gopalswamy 2011). The origin and propagation of moving type IV bursts are still speculated and under review, for example, the association with type II burst occurrences, where type IV bursts follow type II bursts (Robinson 1978; Pick & Vilmer 2008), and are associated with solar eruptions such as flares and CMEs.

Continuous emission known as drifting type IV emission is caused by a source moving outward at a speed of $100 - 1000 \sim \mathrm{km\,s^{-1}}$ across the solar corona (Dulk 1985), very similar to the speed of CMEs (White 2007), or they may originate within dense structures like prominences (Aurass et al. 1999; Bastian et al. 2001; Klein & Mouradian 2002; Bain et al. 2014). They can sometimes be observed at frequencies lower than ~ 20 MHz (DH wavelengths) in the IP space (Hillaris et al. 2016), and they are then called IP type IV bursts.

2.6.5 Type V radio burst

Type V radio bursts appear as a short-duration continuum at meter wavelengths in dynamic spectra (Wild et al. 1959b,a), following type III radio bursts. These bursts are short-lived, lasting around 40 to 200 seconds and decrease in frequency, as reported by Dulk et al. (1980). They originate from the same active region as associated type III bursts, with processes that involve electron streams (Wu et al. 2000, 2002). While the polarization of type V radio bursts is generally low, they often exhibit the opposite polarization to the associated type III bursts (Dulk et al. 1980). Additionally, source displacement is correlated with this polarization reversal (Winglee & Dulk 1986).

3 Observations and data analysis

The data analyzed in this thesis come from various spacecraft and ground-based telescopes. Additionally, *in-situ* observations have been used in particle analysis. The main goal is to use all the available observational data to create a comprehensive picture of the events and answer scientific questions about the acceleration of electrons. This chapter briefly introduces the different spacecraft and instruments onboard, then explains how the data was collected and the methods used to analyze the radio bursts and shock properties.

3.1 Instruments

3.1.1 SOHO

SOHO (Domingo et al. 1995) was launched on 2nd December 1995 and it carried a set of three "coronagraph" telescopes, LASCO C1, C2, and C3 (Brueckner et al. 1995), located at L1 distance. A coronograph is a special optical telescope invented by Lyot (1930) to study the outer corona by creating an artificial solar eclipse with an occulting disk to cover the bright solar disk (Brueckner et al. 1995). Each coronograph has a distinct field of view with some overlap. The C1 coronagraph, which failed in 1998, covered heliocentric distances of $\sim 1.1\,R_\odot$ up to $\sim 3\,R_\odot$. To cover larger distances $\sim 1.5 - 6\,R_\odot$, the second camera, C2 coronagraph (Brueckner et al. 1995) was designed and operated, however, the occulting disk causes diffraction, setting the practical lower field of view limit of C2 to $\sim 2.2\,R_\odot$. The third coronograph, named C3, has the largest field of view from $\sim 3.7 - 30\,R_\odot$. The cadence of LASCO images is in the order of minutes. To enhance certain coronal structures, we can create "running difference" images which are created by subtracting two successive images from each other or provide "base difference" images which are the result of subtracting the start time image from all subsequent images. SOHO/LASCO C2 and C3 running difference images were a part of our data analysis in **Paper I, II, III**.

3.1.2 SDO

The Solar Dynamics Observatory (SDO) (Pesnell et al. 2012) was launched on February 11, 2010, consisting of three instruments on board. The Atmospheric Imaging Assembly (AIA) (Lemen et al. 2012) is designed to take images of the solar corona

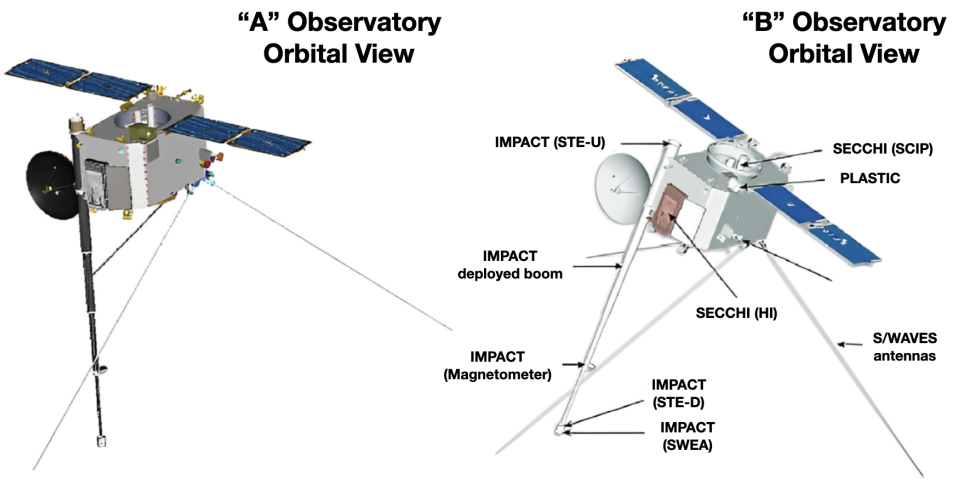

Figure 11. Schematics for the STEREO-A and STEREO-B spacecraft with the instruments on board, adapted from `https://www.eoportal.org/satellite-missions/stereospacecraft`

and transition region up to 0.5 $R_\odot$ above the solar limb, with filters in 10 different wavelengths every 10 seconds. The Helioseismic and Magnetic Imager (HMI) (Scherrer et al. 2012) purpose is to investigate the evolution of magnetic activity and the origin of solar variability. The Extreme Ultraviolet Variability Experiment (EVE) (Woods et al. 2012) aim is to measure the solar EUV irradiance from the full disk of the Sun and its corona in 1 to 1050 Å. Combining data from SDO with information provided by other satellites like STEREO, SOHO, and Wind allows us to investigate the processes that result in energy release and the initiation of solar eruptions in the corona. This, in turn, leads to a better understanding of the origin and evolution of magnetic structures. The SDO/AIA and SDO/HMI images were used in **Paper I**, as part of the analysis of DH type IV radio bursts.

3.1.3 STEREO

The Solar TErrestrial RElations Observatory (STEREO), consisting of twin spacecraft mission (Kaiser et al. 2008), was launched on October 26, 2006. The separation angle between the two spacecraft increases by approximately 45 degrees per year. One of the main goals of this mission is to enhance our knowledge of the initiation mechanisms of CMEs and characterize their propagation into the inner heliosphere and to Earth, and investigate the SEP acceleration mechanisms in the low corona and IP space. In addition, the mission aims to develop and study the plasma parameters and magnetic structures by comparing 3D models with imaging observations.

To achieve the mentioned goals, both STEREO spacecraft consist of four sets of measuring instruments with at least 18 individual sensors to characterize the CME plasma from the solar corona to Earth's orbit. It is important to note that one of the two spacecraft, STEREO-B, was unfortunately lost in 2014. Despite this setback, STEREO-A continues its mission. All four sets of instruments were utilized in our data analysis for all original publications.

- **Sun–Earth Connection Coronal and Heliospheric Investigation (SECCHI)**:

  SECCHI is named after Angelo Pietro Secchi (1818 – 1878), the first astrophysicist to record solar eclipses. It is a package of four scientific telescopes, including two white-light coronagraphs (COR1 and COR2), an EUV imager (EUVI), and a heliospheric imager, to reconstruct a three-dimensional description of the origin and evolution of the CME into the IP medium. (Howard & SECCHI Team 2007). The corresponding coronagraph and EUV difference images were used in **Papers I, III**.

- **In situ Measurements of PArticles and CME Transients (IMPACT)**:

  IMPACT focuses on measuring solar wind and superthermal electrons, IP magnetic field, and SEPs, to study the space weather event correlation and the energetic particle acceleration and propagation mechanisms (Kaiser et al. 2008; Luhmann et al. 2008). Among the seven instruments on IMPACT, three instruments are located on the anti-sunward deployed boom: The Solar Wind Electron Analyzer (SWEA) (Sauvaud et al. 2008), the Suprathermal Electron Instrument (STE) (Lin et al. 2008) and the Magnetic Field Experiment (MAG) (Acuña et al. 2008). The remaining instruments are the Low Energy Telescope (LET) (Mewaldt et al. 2008), the high-energy telescope (HET) (von Rosenvinge et al. 2008), the Suprathermal Ion Telescope (SIT) (Mason et al. 2008) and the Solar Electron and Proton Telescope (SEPT) (Müller-Mellin et al. 2008), located on the main body of STEREO and measuring SEPs.
  For investigating the role of IP shocks during electron ESP events in the range of MeV energies, we used electron and proton flux data measured by HET. The time-intensity profile of relativistic electrons in three energy channels and protons in four energy channels was analyzed for 587 IP shocks in the list [1], to choose significant candidates for electron ESP events in **Paper IV**.

- **PLAsma and SupraThermal Ion Composition (PLASTIC)**:

  In PLASTIC, particles are continuously tracked at a distance of 1 AU, and magnetic fields are constantly measured. CME IP properties are measured with PLASTIC as they pass by the STEREO observatory. The combination

[1] https://stereo-ssc.nascom.nasa.gov/data/ins_data/impact/level3/STEREO_Level3_Shock.pdf

of these measurements with modeling and theory allows us to examine the correlation between solar and IP events (Forbes et al. 2006; Aschwanden et al. 2008). In this thesis, we used the in-situ measurement of bulk properties of solar wind protons at the time of IP shock crossing in **Paper IV**.

- **STEREO/WAVES (S/WAVES)**:

  In radio astronomy, the long wavelengths from decametric to kilometric, roughly below 25 – 10 MHz, cannot be detected on Earth due to ionospheric cut-off. Particles from the energetic eruptions in the solar corona and IP medium cause different forms of solar radio bursts in the mentioned wavelength ranges. SWAVES is a burst tracker device built to detect and investigate coronal and IP shocks caused by CMEs, by measuring the properties of the IP shocks, and the plasma parameters of the inner heliosphere and magnetic clouds. SWAVES instrument consists of five radio receivers that cover radio bursts in the 16 MHz – 30 kHz frequency range, and it is maintained to detect solar radio bursts of type II and type III and other solar radio emissions. The STEREO/WAVES spectrum profiles were the main part of our study in all **four Papers in this thesis**.

3.1.4 Wind

The goal of three radio receivers of Wind/WAVES (Bougeret et al. 1995) is to provide a comprehensive study of radio and plasma wave events in the frequency range from ~ 14 MHz to ~ 3 kHz. Therefore, it can detect radio emissions below Earth's ionospheric limit and provide similar data to STEREO/WAVES. The Wind/WAVES dynamic spectrum along with the STEREO/WAVES were the main part of our study in the **Papers I, II, and III**. The analyzed events were selected from the Catalog of radio type II and IV bursts, produced by Michael L. Kaiser [2].

3.1.5 GOES

The X-ray Sensor (XRS) (Thomas et al. 1985; Garcia 1994) is an instrument on board *Geostationary Operational Environmental Satellite (GOES)* which is designed to measure the X-ray intensity of flares, developed in 1970. The classification of flares (i.e., GOES class) is based on the observed flux in the soft X-ray spectral band of 1-8 Å. The letters A, B, C, M, and X define the order of magnitude of the peak flux, from the weakest to the strongest, respectively. Table 1 provides a brief overview of the classes and their associated flux magnitudes. The number associated with each letter is the flux magnitude's mantissa in the exponential representation.

[2] https://spdf.gsfc.nasa.gov/pub/data/stereo/documents/websites/solar-radio/wind/data_products.html

Table 1. Solar flare classification

Soft X-ray class	
class	Flux [W m^{-2}]
A	10^{-8} – 10^{-7}
B	10^{-7} – 10^{-6}
C	10^{-6} – 10^{-5}
M	10^{-5} – 10^{-4}
X	$> 10^{-4}$

For example, X3.2 is an X-class flare with a flux magnitude of 3.2×10^{-4} W m^{-2}. In this case, "3.2" is the mantissa, and "10^{-4}" is the exponent. GOES soft X-ray data related to the analyzed events were used in the **Papers I, II and, III**.

3.1.6 Ground-based radio telescopes

- **Nançay Radioheliograph (NRH)**:

  NRH (Kerdraon & Delouis 1997) is the only instrument that provides regular European daytime imaging of the solar corona, up to half the solar radius above the Sun's surface. The NRH provides thousands of interferometric 2D images of the Sun at frequencies between 150 – 450 MHz with a cadence of 8 images/second. NRH images that identify the location of the radio emission source at 164 MHz are used in **Paper II**.

- **Nançay Decameter Array (NDA)**:

  NDA is a radio telescope built between 1975 and 1977 to observe at frequencies from 10 MHz to 80 MHz. It is used to collect high-resolution dynamic spectra of intense radio sources that appear as decametric radio emissions. The new spectrograph named ORPHEES was integrated into the array in 2011 and covers the frequency band of 100 MHz to 1 GHz. The radio dynamic spectra observed by the NDA at 70 – 10 MHz were used to identify the location of the flare region and detect the type IV metric radio burst in the **Papers I, II** [3].

- **Green Bank Solar Radio Burst Spectrometer (GBSRBS)**:

  The Solar Radio Burst Spectrometer (SRBS) is located in the Green Bank (GB) site of the National Radio Astronomy Observatory, to provide high-quality radio dynamic spectra in the UT time range of 12 – 24. The spectrometer supported observations at 20 – 1050 MHz with a time resolution of approximately

[3] `https://secchirh.obspm.fr/`

1 second. GBSRBS data are available up to July 2012 (White et al. 2005; Bastian et al. 2005; Bradley et al. 2005). Three metric type IV continuum emissions observed by GBSRBS dynamic spectra at 20 – 70 MHz are part of our analysis in **Paper II**.

- **Radio Solar Telescope Network (RSTN)**:

  Radio Solar Telescope Network (RSTN), is a global network of solar radio observatories, controlled by the United States Air Force. The observatories are located at different sites around the world and monitor solar radio emissions by taking dynamic spectra in the range of 25 – 180 MHz. We used the dynamic spectrum observed by Learmonth Station to check the metric type II burst in **Paper III**, and San Vito and Palehua stations in **Paper II** to analyze the metric type IV burst [4].

[4] https://www.ngdc.noaa.gov/stp/space-weather/solar-data/solar-features/solar-radio/rstn-spectral/

3.2 Data analysis

3.2.1 Radio bursts

Solar eruptions act as accelerators of energetic particles into the inner heliosphere through various mechanisms. Solar radio bursts are powerful and available tools for studying the origin and trajectory of particles across a broad wavelength range, from meter to kilometer waves. The classification of radio bursts, as a consequence of the acceleration of nonthermal electrons, may depend on the emission mechanisms or the source of the emission, which, in this context, are electrons (Wilson et al. 2009).

The various radio emission mechanisms appear in nearly all phases of solar eruptions. They can be either coherent or incoherent (e.g., Melrose 2017; Nindos 2020), and the electron distribution can be classified as thermal or non-thermal (e.g., Condon & Ransom 2016), depending on the energy and velocity. The two most important incoherent emission mechanisms on the Sun are free-free or bremsstrahlung and gyromagnetic emission. The summation of individual electron radiation produces incoherent emission. However, coherent emission is generated when electrons emit together, acting as a one-unit.

Free-free radiation, originating from thermal electrons, is responsible for radio emissions from both the quiet Sun (Nindos 2020) and the expanding trapped coronal plasma in a magnetic field from the Sun. This emission from thermal electrons is hard to observe because the brighter emission from non-thermal sources can conceal it (Vourlidas 2004). By moving an electron in a magnetic field, it experiences a force that causes acceleration, and as a result, the accelerating charged particle emits electromagnetic radiation continuously. According to Lorentz's law, expressed as

$$\mathbf{F} = -e\mathbf{V} \times \mathbf{B}$$

the force depends on the charge of the electron, velocity, and magnetic flux density. Gyromagnetic emission (Nindos 2020) term belongs to the radio emissions caused by moving electrons in a magnetic field and is divided into three groups based on emitting energy. Gyroresonance or cyclotron emission for non-relativistic electrons. Gyrosynchrotron emission belongs to the near-relativistic electrons, and synchrotron emission occurs when electrons are in the relativistic energy range (Dulk 1985).

An example of a coherent emission is plasma emission which is a dominant mechanism in solar radio emissions at frequencies less than 1 GHz (Aschwanden 2004), and the main source of radio bursts associated with CMEs (Vourlidas 2004, see Fig. 12). The emission mechanism near the fundamental and harmonic frequencies of type II radio bursts is plasma emission. The shock-accelerated electron beams in the foreshock excite Langmuir waves (Cairns et al. 2003). The relation between the frequency f_p (Hz) and electron density n_e (cm^{-3}) at the fundamental is introduced by

$$f_p = 9000\sqrt{n_e}.$$

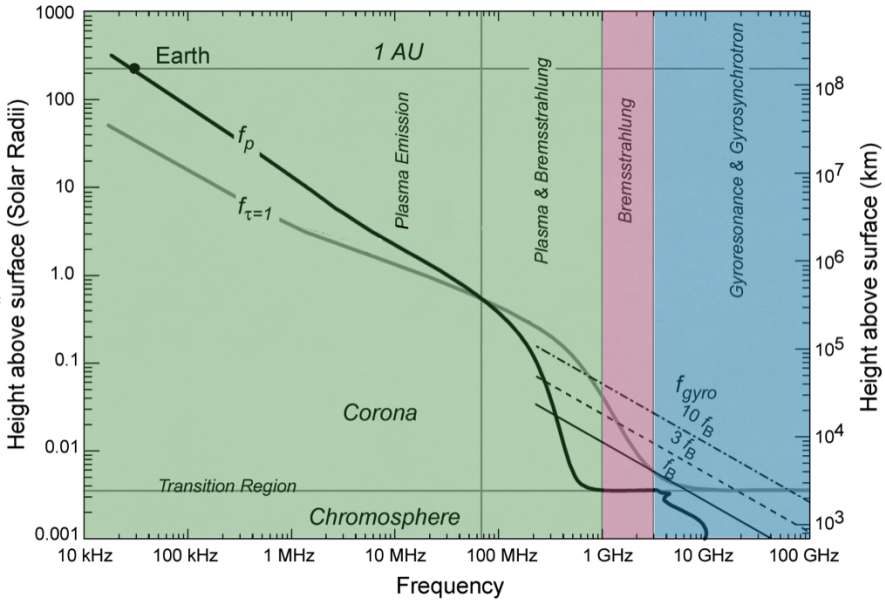

Figure 12. Based on the top curve in this plot, emission mechanisms at various frequencies within the solar atmosphere can be determined (Krüger 1984). The $f_\tau = 1$ is the frequency at which free-free emission becomes optically thick. Three lines – $f_B, 3f_B, 10f_B$ – are shown for gyroemission (the cyclotron frequency and its harmonics). The curves are based on the different models of the plasma parameters such as temperature, density (Vernazza et al. 1981), and strength of magnetic field (Dulk & McLean 1978). The plot covers seven orders of magnitude in frequency and height above the surface of the Sun. Adapted from Gary & Hurford (2004).

This relation is used to interpret the height of the radio emission. As the radio source moves, the density of electrons and the frequency of the emitted radio waves decreases at higher altitudes in the solar atmosphere, which means that the lower frequencies are emitted from greater heights. Therefore, the frequency drift of type II burst in the dynamic spectrum can be used as a tool to estimate the shock velocities. However, the appearance of type II emission lanes in the dynamic spectrum is not always clear, and identifying the emission lane can be challenging (Robinson & Stewart 1985). Sometimes the radio bursts show emissions just at the fundamental, and the harmonic emission lane (near $2f_p$) is not visible in the spectrum. Sometimes, on the other hand, type II bursts appear in the dynamic spectrum at very low frequencies, without earlier signatures. These 'isolated' DH type II bursts were studied in **Paper III**, and the aim was to find out if the associated shocks were formed late, or if the appearance of radio bursts was delayed for some reason. The data set included also bursts where we had observations from at least two different viewing angles, allowing us to view the far side of the Sun with the STEREO spacecraft observations. Possible reasons for not observing type II bursts at higher frequencies are that the emission sources start to propagate from the far side of the Sun, and they become visible only when the sources get higher, or that other dense, absorbing regions exist along the lines of sight. Both scenarios were found in the data analysis. Radio emissions may also require particular coronal conditions to form, but this aspect was left out of the study in **Paper III**.

Radio observations can be used to find the shock velocities from the plasma frequencies. The first step is to calculate the electron density from plasma frequency at the fundamental lane of the radio burst. Then atmospheric density models are used to estimate the height of the radio burst emitting source (Robinson & Stewart 1985). Fig. 13 shows how the various atmospheric models cover different parts of the corona to estimate the electron density. The common approximation used for the plasma density in IP space is

$$n_e = n_0/R_d^2$$

where n_0 is the electron density near Earth (ranges $\sim 5 - 50$ cm^{-3}) at 1 AU, and R_d is the distance from the Sun in AU (Reiner et al. 2001).

To estimate the velocity of a CME-driven shock through radio observations, one approach relies on the association with an IP type II radio burst, generated by electrons accelerated near the CME's leading edge at the bow shock. Accounting for a potential offset time between the burst driver and the bow shock (Russell & Mulligan 2002), another consideration would be the accurate determination of the CME height using white light images, although the observed height is influenced by projection effects. The projected CME height is used as a means of evaluating the atmospheric density models, with the selection of models that best align with the CME observations (an example of using this method was done by Ciaravella et al. 2005;

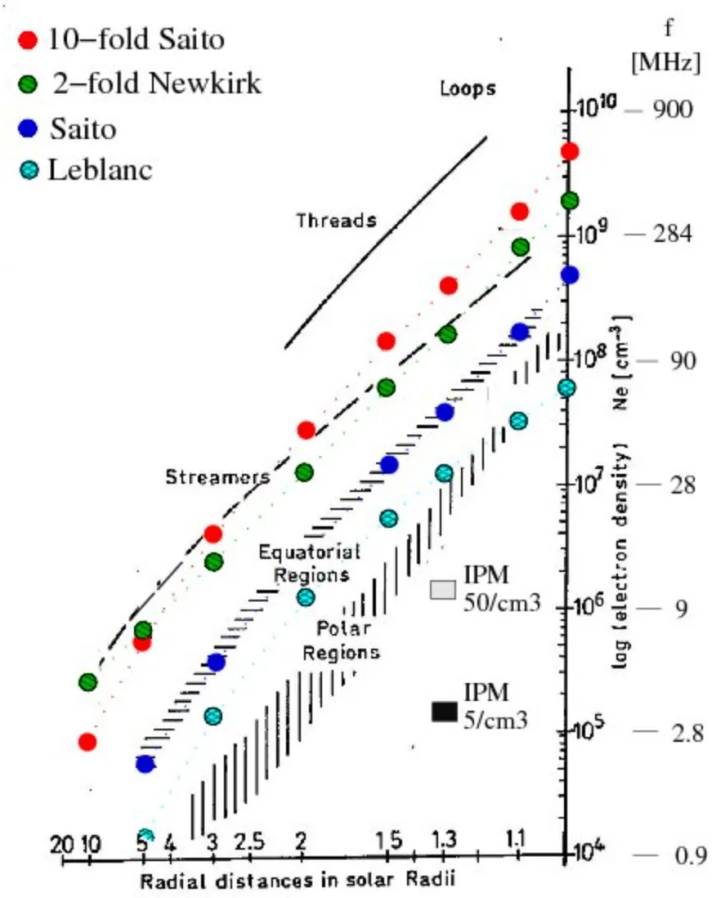

Figure 13. Electron density in different parts of the corona from eclipse photometry, with data points from often used atmospheric density models (Pohjolainen et al. 2007). Coronal densities according to: the Saito et al. (1977) model (dark blue circle), the ten-fold Saito model (red circle), the two-fold Newkirk (1961) model (green circles) and the Leblanc et al. (1998) model (light blue circles). The IPM-labeled boxes refer to the IP density model at 1.3 solar radii, with near-Earth electron densities of $5/cm^3$ (solar minimum) and $50/cm^3$ (solar maximum). Adopted from Pohjolainen et al. (2007).

Pohjolainen et al. 2007). This method connects bursts in the corona and IP space using different density models. When the burst driver propagates radially along the density gradient, the observed velocity is assumed to represent the shock velocity. However, deviations in their directions lead to an increased actual velocity. In most cases, the propagation direction is along the radial decrease of the density.

Another method involves measuring shock speeds at decimetric wavelengths using the observed frequency drift rate and the density scale height. The expression for shock velocity (υ) is given by

$$\upsilon = 2\frac{1}{f}\frac{df}{dt}H$$

where f is the observing frequency (fundamental emission) in MHz and $\frac{df}{dt}$ is the frequency drift obtained from a logarithmic spectral plot, and H is the density scale height, expressed in km by:

$$H = \left(\frac{1}{n}\frac{dn}{dr}\right)^{-1}.$$

This method is based on differentiating the plasma frequency and electron density and using the relation $f = \sqrt{n}$.

Type IV radio bursts with a frequency of less than 15 MHz are less common compared to types II and III radio bursts in this frequency range. Radio emissions of type IV mostly originate at metric wavelengths and extend downward to approximately 6 – 9 MHz, where they become detectable using instruments like Wind/WAVES and STEREO/WAVES. During the time, when the magnetic cloud lifts off from the surface of the Sun, the emission mechanisms of type IV radio bursts could be both gyrosynchrotron and plasma emission. Tracking the evolution of IP type IV bursts and their characteristics, in relation with flares and CMEs between 1998 and 2012, were studied by Hillaris et al. (2016). It is a comprehensive study of IP type IV bursts recorded by Wind/WAVES in the 14 MHz – 20 kHz frequency range, and by many ground-based observatories in meter and decameter wavelengths. Most of the compact type IV radio bursts with long duration were associated with M and X class flares and CMEs faster than 1000 km s^{-1}.

Directivity of moving type IV bursts was introduced by Kundu (1965). His theory for type IV directivity was the extent of the source. The source size appears larger when viewed on top, in the direction of propagation, and smaller when viewed from the side. This research topic was not given much attention until Gopalswamy et al. (2016) analyzed an IP type IV radio burst that occurred in 2013 and was observed by multiple spacecraft, including Wind, STEREO-A, and STEREO-B. The intense type IV burst was partially observed by STEREO-A, completely observed by STEREO-B, but not detected by Wind close to the Earth. The work also included statistical analysis of a large sample of type IV radio bursts observed with

Wind/WAVES during solar cycle 23 (1996-2008). They suggest that type IV bursts are fully and intensely observed when they originate and are directed within a cone of 60 degrees or less above the source origin. In addition, the study confirmed that the events that originated near the disk center always appeared complete. Typical IP type IV burst is associated with an EUV wave and is often followed by fast CME and IP type II bursts (Pohjolainen & Sheshvan 2018).

In the following step, our motivation was to study IP type IV burst directivity further, with data from the three spacecraft at times when the full 3D view of the Sun was available. The time period was set to 2011 - 2012, as then the separation was approximately 90 degrees between each spacecraft. The far side of the Sun could also be imaged in EUV and white-light. Our results were presented in **Paper I**, in a study of five compact IP type IV radio bursts that had full data coverage. We analyzed features in the radio dynamic spectra, along with the white-light and EUV images, to find out their source origin and possible directivity effects.

All the analyzed type IV radio bursts in this study were associated with fast CMEs (based on SOHO/LASCO CME catalog, Gopalswamy et al. 2009) and type II radio bursts. By calculating the height of type II and type IV emission using the density model of Vršnak et al. (2004) and the CME leading front, the height separation of type IV and the propagating type II shows that a shock was located at the CME flanks, and not due to a bow shock. Using radio triangulation to locate the position of the type II radio source in Magdalenić et al. (2014) shows that the signature of the radio source was located close to the CME flank, and therefore the interaction of the shock wave and the coronal streamer produced an IP type II radio burst. The termination of type III radio bursts close to the type II frequencies, as reported by Al-Hamadani et al. (2017), could be attributed to the depletion of radio emission by intersecting two electron beams (Briand et al. 2014), or the halting of penetration due to the dense type II-streamer region. These diverse findings led to explaining the directivity characteristic of IP type IV bursts as due to absorption. For example, the dense plasma toward a certain viewing angle could block the emission at longer wavelengths. High-density plasma could be formed around shock-streamer interaction regions or near the CME front or flanks that show up as type II radio emission (**Paper I**).

Moving type IV radio bursts do not show a directivity effect like stationary type IV but sometimes show partial cut-off features in the dynamic spectrum (Paper II). In this study we extended the frequency range to decameter waves and also included ground-based radio imaging. The conclusion was similar to the conclusions in **Paper I**, that either absorption or suppression of emission was the cause for cut-offs, as increased plasma density in streamers or shock-related regions existed toward the line of sight.

The research on type IV bursts has since continued to examine their fine structures and sources of emission, using mostly ground-based radio observations. For

example, in their case study Melnik et al. (2018) concluded that the source of the burst is the core of the CME and this emission can be observed at decameter waves. As STEREO spacecraft positions have changed, no longer giving a 3D view, and STEREO-B has not provided data since 2014, the studies of type IV emission directivity have been sparse.

3.2.2 Particles

The Sun is capable of accelerating particles to high energies through various transient events. The processes leading to the acceleration and propagation of particles are generally relevant to astrophysical plasma. An extra benefit of the Sun is that the evidence of non-thermal particles, like their electromagnetic emissions and measurements in space, are easily available. The acceleration and propagation of SEPs from their source to the observer in IP space have been studied by in-situ observations from space and ground-based observations. The focus of this thesis is on the transport and acceleration processes of electrons in IP space.

Previous studies confirmed that magnetic reconnection as a possible mechanism in solar flares can accelerate electrons up to relativistic energies (e.g., Mann 2015). However, the role of shocks driven by CMEs as other acceleration mechanisms remains a subject of ongoing discussion. The existence of radio burst features in dynamic spectra, along with the particle intensity profile, offer evidence of accelerating mechanisms for various populations of non-thermal electrons traveling in the corona and IP space (see, Nindos et al. 2008; Klein 2021a,b).

A shock wave is the topic of interest in this thesis and is an example of a boundary in plasma, caused by the movement of a disturbance through the plasma with a speed higher than the local magnetosonic speed. CME-driven shocks are collisionless shocks. When CMEs propagate through the heliosphere and are detected by in-situ spacecraft at 1 AU, the first feature in spacecraft data is a CME-driven IP shock, since approximately half of the ICMEs are accompanied by shocks (Lepping et al. 2015). IP shocks represent abrupt discontinuities (Priest 2014) in the intensity and plasma conditions profile by sudden passage between the undisturbed (upstream) and disturbed (downstream) parts of the plasma.

Three main modes of propagation of Magnetohydrodynamic (MHD) waves are often used to approximate the fundamental characteristics of shock waves. Fast, slow, and intermediate shocks are distinguished by their different conditions and by their Mach number (Oliveira 2017), which is defined how fast the shock is compared to the medium. CME-driven shocks are classified as fast shocks (Kivelson & Russell 1995). Shock strength can also be determined by Alfvénic Mach number M_A, which is determined by Alfvén speed V_A (Priest 2014; Oliveira 2017). In this thesis, we consider IP shocks with Alfvénic Mach numbers larger than 1. The angle between the shock normal and the upstream magnetic field is θ_{Bn}. The orientation of the shock front in relation to the upstream magnetic field plays an important role in classifying shocks and influencing particle acceleration at the shock front.

Increasing energetic particle intensities at the time of the IP shock passage are called ESP events (Bryant et al. 1962; Rao et al. 1967). The two categories of ESP events are spike and classic ESP events, reported by Sarris & van Allen (1974). The spike events are followed by the shock drift acceleration theory at quasi-perpendicular

shocks. The classical ESP events last for several hours, and are produced by diffusive shock acceleration at quasi-parallel shocks, and can appear on two sides of the shock (upstream and downstream regions).

The occurrence of ESP events and their correlation with other events like IP shocks, CMEs, type II radio bursts, and SEP events have been investigated in several studies. The time-intensity proton profile has been investigated in broad energy ranges during ESP events (Dresing et al. 2016; Mäkelä et al. 2011; Ameri et al. 2023). Ameri et al. (2023) analyzed the proton enhancements at energies higher than 1MeV and found that most of the IP shocks are associated with ESP events. In addition, the peak intensities of ESP events correlated with shock transit speeds, together with the appearance of DH type II radio bursts and SEP events.

3.2.3 Magnetic field

The package commonly used for simulation and visualization of the solar coronal magnetic field is the so-called Potential Field Source Surface (PFSS) model (Schatten et al. 1969; Hoeksema 1984; Wang & Sheeley 1992). The PFSS model uses a global radial Carrington synoptic map to achieve a configuration of the coronal magnetic field and the main assumption of the model is that the electric current in the corona is zero. The periodicity of the direction of the IP magnetic field is 27 days and is well correlated with the direction of the photospheric magnetic field (Ness & Wilcox 1964). In addition, since most of the coronal field is Maxwell stress-free, the PFSS model gives an acceptable estimate of resolving global structures on spatial scales. For comparing different models of the coronal magnetic field, see e.g., Neugebauer et al. (1998); Riley et al. (2006).

The PFSS maps were used in **Papers I and III** to approximate the structure of magnetic fields over the active region in these events. The open field lines in PFSS maps estimate the locations where accelerated particles can propagate and appear as type III radio bursts in the dynamic spectrum (Fig. 2 in **Paper I**).

4 Summary of the original publications

4.1 Paper I

Visibility and Origin of Compact Interplanetary Radio Type IV Bursts

In this article, we have analyzed five compact DH type IV radio bursts from a time period of two years, 2011-2012. The events were selected from a catalog of type II and type IV solar radio bursts prepared by Michael L. Kaiser. Using SDO and SOHO images for the Earth side, and EUV and white-light images on board the STEREO-A and-B spacecraft, we got a full 3D view of the Sun as the spacecraft have $\approx 90^{\circ}$ angular separation from each other. Two of the DH type IV bursts did not have radio and X-ray observations at lower heights, since they originated from the backside of the Sun.

All our events were associated with EUV waves. However, those with strong type IV emission in dynamic spectra show the wave across the whole visible disk, and those with low intensity and cut-off features have EUV waves that are visible only near the limb. The listed CMEs and type II radio bursts linked to the five events show that all CMEs had high speeds around the onset time of type IV burst. Using the atmospheric density model of Vršnak et al. (2004), the spatial difference between the propagation of type II shock and the type IV source was around 4-9 $R_{\odot}$.

This study aims to understand the situation that leads to the type IV radio burst to be observed from a specific direction. Kundu (1965) brought up the idea of the directivity of type IV radio bursts. Later studies (Gopalswamy et al. 2016; Melnik et al. 2018) analyzed different cases of type IV radio bursts and suggested that the emission mechanisms or the location of the energy source for the bursts could be the reason for directivity. However, we note that it is also possible that the local density enhancements could be blocking the radiation to a defined direction. CME shock front or coronal streamers are such regions with higher density (Kwon & Vourlidas 2018), presented in all five cases studied in this article.

The spectral analysis of our events shows the existence of a type II radio burst toward the direction where type IV burst is not visible or is partially visible. To sum up the analysis, the existence of high-density regions like streamers, shocks at the CME flanks, and at higher locations with dense regions in the corona, confirm the blocking scenario in our event list.

4.2 Paper II

Cut-off features in interplanetary solar radio type IV emission

This paper covered three separate type IV radio bursts at decameter wavelengths originating from the same active region on 23, 25, and 29 July 2004. The analysis continues the study of the reasons for the directivity of type IV radio bursts.

These events were associated with flares, CMEs, and type II radio bursts. Throughout the Sun's rotation, the active region moved from the disk center to the west limb during this time interval. This allowed us to track the features along the rotation time. We used spectral data from Wind, RSTN, GBSRBS, NDA, and images from NRH to confirm the source locations of the radio bursts.

Plasma emission is the most common radio emission mechanism for trapped particles in propagating plasma structures, although synchrotron emission cannot be ruled out in the case of type IVs. At the local plasma frequencies, accelerated particles in type II bursts show emission at fundamental and harmonic lanes. We directly defined the density of the local plasma by measuring the emission frequency, and then we estimated the emission source height by using atmospheric density models (Pohjolainen et al. 2007; White 2007).

The fine structures inside these three type IV bursts include repeated type III-like bursts that show particle acceleration along magnetic field lines, with opposite directions of frequency drift at metric wavelengths. Nevertheless, the presence of specific patterns was challenging to confirm due to the low resolution of the radio spectral data. The density of radio emission patterns inside the metric type IV is weakest for the event on the limb. Images from NRH at 164 MHz were used to indicate the location of the radio source and the heliocentric distance, to recognize the emission mechanisms.

In the first event, we have a "full" type IV radio burst in the dynamic spectrum (i.e., no cut-offs in emission) from an event located near the disk center, as well as a short type II radio burst which ended just before type IV emission. The type II likely occurred because of a shock at the flank of the first CME, or due to a bow shock of the following, later CME.

For the second event, with the source location at W30, we have two separate type II radio bursts with partial cut-off emissions in the moving type IV burst. Higher plasma density regions like at the CME flanks and bow shock regions as well as streamers, were the most feasible spots for the formation of type II radio bursts. Therefore, reduced emissions in these events could be the result of absorbing or suppressing the emission on a specific viewing angle by a denser plasma medium. The third, a limb event, also had the same pattern in the dynamic spectrum.

4.3 Paper III

Formation of Isolated Radio Type II Bursts at Low Frequencies

In this paper, we present the results of a statistical analysis of flare and CME characteristics that produce the *"isolated"* type II radio bursts, observed in 1998-2016. Isolated events happen without simultaneous or earlier radio emissions. The events were selected from the list provided by Gopalswamy et al. (2019).

We performed a statistical and correlation analysis of the events that showed variability in bandwidth, duration, and harmonic content. The analysis shows that the source origin of these kinds of bursts is not in the central meridian between 0 - 30 degrees east or west. All 26 isolated type II bursts were associated with a shock driven by a CME. However, analysis suggests that a CME bow shock is more common than a flank shock, as the bursts are well separated from other radio signatures. The time delay in the appearance of DH type II burst in the dynamic spectrum could have different reasons:

- Eruptions occur on the far side of the Sun and the emission source needs time to get high enough to be observed.
- Existence of high-density plasma regions like a streamer or earlier CME fragments in the observed direction. These dense areas act as an occulting structure, with a higher plasma frequency.
- Sensitivity issue of observations by different satellite instruments.

The CME speeds in the analyzed cases were mostly higher than the local Alfvén speed (Kim et al. 2012), and they satisfy the essential conditions for the occurrence of a DH type II burst by coronal shocks. As a result of this study, the isolated DH type II radio burst could be a branch of DH type II bursts. Therefore, the emission region needs to have peculiar coronal conditions compared to other shocks (Ganse et al. 2012). The other recent study by Annenkov et al. (2020) also supports the theory of a specific condition of the local environment.

4.4 Paper IV

On the role of interplanetary shocks in accelerating MeV electrons

We selected 27 potential electron ESP events to be analyzed by scanning the whole STEREO mission between 2007-2019 and checking the monthly intensity plots of HET observations together with the STEREO list of whole 587 IP shocks provided by Jian et al. (2013). The well-studied ESP events propagating through the IP space around CME-driven shocks have several reports about the ability to accelerate protons in a wide range of energy from keV to tens of MeV (references in paper IV). This study aims to investigate the ESP event at the time of the IP shock passing by the STEREO spacecraft and the role of IP shocks in enhancing the electron intensity to MeV energies at 1 AU.

Although the effects of IP shocks in the enhancement of proton intensity at the time of in-situ shock passage at spacecraft are well-established in previous studies, there is still doubt about the same with respect to electron acceleration. However, the study of Dresing et al. (2022) gives the motivation to analyze the high-energy electron observations at the time of IP shock, since these authors found a good correlation between the electron peak intensity and the Mach number of the coronal shock.

The HET instrument has three energy channels to measure the electrons, from 0.7 to 4.0 MeV. Firstly, checking the reality of electron enhancement in the events is important since ion contamination may be an issue in the low-energy channels. Additionally, the potential influence of mixed features, such as type III burst occurrences before shock crossing, infers the presence of another SEP event or solar eruption, which may contribute to electron acceleration. The new filtering method introduced in this paper is a good way to identify the local variation of the particle intensity profile.

The result of using the filtering technique is nine electron ESP events that showed a significant peak in the time-intensity profile associated with ICME-driven shock and a shock transit speed of more than 900 km/s. Since the electron ESP events sometimes do not have a clear peak around the shock crossing time, we classified them unlike the previously categorized ESP events by Sarris & van Allen (1974). Based on the characteristic behavior of the events around the shock crossing time, we divided them into plateau, peak, and plateau + peak events. In conclusion, in-situ observation exhibits clear signatures of local acceleration of electrons by IP shock or ICME's sheath region during the ESP event. However, these events are still rare to happen at 1 AU, and it seems that special conditions are needed for their creation. This indication could be supported by the frequent presence of several CMEs/shocks around the time of the studied shock.

4.5 The author's contribution to the publications

Paper I. Visibility and Origin of Compact Interplanetary Radio Type IV Bursts

Contributed to the research idea and selected DH type IV radio burst events. Performed the data analysis of the events and prepared the majority of the figures. Made substantial contributions to the writing of the text and actively participated in the interpretation of the results.

Paper II. Cut-off features in interplanetary solar radio type IV emission

Contributed to the spectral and timing analysis of both ground and space-based observations. In charge of preparing the dynamic spectra and other figures and participated in the interpretation of the results.

Paper III. Formation of Isolated Type II Bursts at Low Frequencies

In charge of the majority of spectral and correlation analysis. Contributed to the writing of the manuscript and approach of the study.

Paper IV. On the role of interplanetary shocks in accelerating MeV electrons

Compiled and analyzed the data obtained by STEREO/WAVES and STEREO/HET and prepared all figures and tables. The majority of the manuscript was written by the author.

5 Conclusions and outlook

In this dissertation, I have investigated the radio signatures of electron acceleration by analyzing the dynamic spectra provided by various spacecraft, to determine the source origins of type II and type IV radio emissions. The other part of the study focuses on the role of CME-driven shocks in accelerating electrons to MeV energies, utilizing in-situ observations of shock-accelerated electrons associated with CMEs. Analysis of fast halo-type CMEs revealed that strong IP type IV radio bursts occur when EUV waves are observed to propagate globally. The study suggests that directivity effects in these events may be due to absorption, which is potentially caused by higher-density plasma at radio type II burst shock fronts. The absorption hypothesis indicates the possibility of reduced emission towards certain viewing angles. Type II bursts were likely created by shock-streamer interactions, with streamers being high-density plasma regions in the corona. The study concludes that observing a type IV burst from the solar disk center could show the CME propagation direction. However, if directivity is caused by absorption/blocking, it illustrates the formation of high-density regions within the CME structure.

Since most type II bursts occur in connection with other types of radio emissions, some isolated DH type II bursts could be associated with CME lift-off on the far side of the Sun, as their emission would be observed only when the source reaches a sufficient height in the solar atmosphere. Additionally, this research suggests a special subgroup within DH type II bursts, due to isolated DH type II bursts dependence on specific coronal conditions.

In parallel, the filtering method I developed in the analysis of in-situ observations successfully isolated nine IP shocks associated with local acceleration of relativistic electrons that were identified out of 27 electron ESP event candidates from STEREO mission data. This study classified electron ESP events based on time-intensity profiles. All nine cases were linked to shocks from IP CMEs with high transit speeds exceeding 900 km/s. Detailed analysis of three events, including two associated with SEP events and one isolated ESP event, revealed complex ICME structures and interactions in IP space. Gradual SEP events show a strong association with DH type II bursts. Conversely, the occurrence of electron ESP events, corresponding to preceding SEP events, is rarer compared to DH type II bursts. This consistency aligns with the concept that DH type II bursts are generated by electrons of considerably lower energies than the MeV range.

To extend this research, future studies are essential to explore the more gradual contributions of shocks to energetic electron fluxes that the current filtering method may not detect. The upcoming solar maximum, marked by fast CMEs, provides an opportunity for more precise identification of electron events by using the enhanced observational instruments on board Solar Orbiter and Parker Solar Probe. Investigating the signatures of energetic electrons through radio emissions and direct spacecraft observations, coupled with utilizing particle acceleration models, can enhance our understanding of electron acceleration by IP shocks.

List of References

Acuña, M. H., Curtis, D., Scheifele, J. L., et al. 2008, Space Sci. Rev., 136, 203

Al-Hamadani, F., Pohjolainen, S., & Valtonen, E. 2017, Sol. Phys., 292, 127

Ameri, D., Valtonen, E., Al-Sawad, A., & Vainio, R. 2023, Advances in Space Research, 71, 2521

Annenkov, V. V., Volchok, E. P., & Timofeev, I. V. 2020, ApJ, 904, 88

Appleton, E. & Hey, J. S. 1946, Philosophical Magazine, 37, 73

Aran, A., Agueda, N., Afanasiev, A., & Sanahuja, B. 2018, in Astrophysics and Space Science Library, Vol. 444, Solar Particle Radiation Storms Forecasting and Analysis, ed. O. E. Malandraki & N. B. Crosby, 63–78

Armatas, S., Bouratzis, C., Hillaris, A., et al. 2019, A&A, 624, A76

Aschwanden, M. J. 2004, Physics of the Solar Corona. An Introduction

Aschwanden, M. J. 2005, Physics of the Solar Corona. An Introduction with Problems and Solutions (2nd edition)

Aschwanden, M. J., Burlaga, L. F., Kaiser, M. L., et al. 2008, Space Sci. Rev., 136, 565

Aurass, H., Vourlidas, A., Andrews, M. D., et al. 1999, ApJ, 511, 451

Bain, H. M., Krucker, S., Saint-Hilaire, P., & Raftery, C. L. 2014, ApJ, 782, 43

Bastian, T. S., Bradley, R., White, S., & Mastrantonio, E. 2005, in AGU Spring Meeting Abstracts, Vol. 2005, SH43A–16

Bastian, T. S., Pick, M., Kerdraon, A., Maia, D., & Vourlidas, A. 2001, ApJ, 558, L65

Bemporad, A., Sterling, A. C., Moore, R. L., & Poletto, G. 2005, ApJ, 635, L189

Benz, A. O. 1980, ApJ, 240, 892

Benz, A. O. 2017, Living Reviews in Solar Physics, 14, 2

Benz, A. O. & Wentzel, D. G. 1981, A&A, 94, 100

Bougeret, J. L., Kaiser, M. L., Kellogg, P. J., et al. 1995, Space Sci. Rev., 71, 231

Bradley, R., Parashare, C., White, S. M., & Bastian, T. S. 2005, in Astronomical Society of the Pacific Conference Series, Vol. 345, From Clark Lake to the Long Wavelength Array: Bill Erickson's Radio Science, ed. N. Kassim, M. Perez, W. Junor, & P. Henning, 357

Briand, C., Henri, P., & Hoang, S. 2014, Journal of Geophysical Research (Space Physics), 119, 2365

Brueckner, G. E., Howard, R. A., Koomen, M. J., et al. 1995, Sol. Phys., 162, 357

Bryant, D. A., Cline, T. L., Desai, U. D., & McDonald, F. B. 1962, J. Geophys. Res., 67, 4983

Cairns, I. H., Knock, S. A., Robinson, P. A., & Kuncic, Z. 2003, Space Sci. Rev., 107, 27

Cane, H. V. & Stone, R. G. 1984, ApJ, 282, 339

Cane, H. V., Stone, R. G., Fainberg, J., Steinberg, J. L., & Hoang, S. 1982, Sol. Phys., 78, 187

Carrington, R. C. 1859, MNRAS, 20, 13

Chen, B., Shen, C., Gary, D. E., et al. 2020, Nature Astronomy, 4, 1140

Chen, Y. 2013, Chinese Science Bulletin, 58, 1599

Chen, Y., Du, G., Feng, L., et al. 2014, ApJ, 787, 59

Chen, Y., Feng, S. W., Li, B., et al. 2011, ApJ, 728, 147

Cheng, X., Li, Y., Wan, L. F., et al. 2018, ApJ, 866, 64

Chernov, G. P., Fomichev, V. V., Gorgutsa, R. V., et al. 2014, Geomagnetism and Aeronomy, 54, 406

Chernov, G. P., Stanislavsky, A. A., Konovalenko, A. A., et al. 2007, Astronomy Letters, 33, 192

Cho, K. S., Moon, Y. J., Dryer, M., et al. 2005, Journal of Geophysical Research (Space Physics), 110, A12101

Chrysaphi, N. 2021, PhD thesis, University of Glasgow, School of Physics and Astronomy
Ciaravella, A., Raymond, J. C., Kahler, S. W., Vourlidas, A., & Li, J. 2005, ApJ, 621, 1121
Cliver, E. W. 2009, in Universal Heliophysical Processes, ed. N. Gopalswamy & D. F. Webb, Vol. 257, 401–412
Cliver, E. W. & Dietrich, W. F. 2013, Journal of Space Weather and Space Climate, 3, A31
Coles, W. A. & Maagoe, S. 1972, J. Geophys. Res., 77, 5622
Condon, J. J. & Ransom, S. M. 2016, Essential Radio Astronomy
Crosley, M. K. & Osten, R. A. 2018, ApJ, 862, 113
Dauphin, C., Vilmer, N., & Krucker, S. 2006, A&A, 455, 339
Desai, M. & Giacalone, J. 2016, Living Reviews in Solar Physics, 13, 3
Dąbrowski, B. P., Krankowski, A., Błaszkiewicz, L., & Rothkaehl, H. 2016, Acta Geophysica, 64, 825
Domingo, V., Fleck, B., & Poland, A. I. 1995, Space Sci. Rev., 72, 81
Dresing, N., Kouloumvakos, A., Vainio, R., & Rouillard, A. 2022, ApJ, 925, L21
Dresing, N., Theesen, S., Klassen, A., & Heber, B. 2016, A&A, 588, A17
Dulk, G. A. 1985, ARA&A, 23, 169
Dulk, G. A., Gary, D. E., & Suzuki, S. 1980, A&A, 88, 218
Dulk, G. A. & McLean, D. J. 1978, Sol. Phys., 57, 279
Echim, M. M., Lemaire, J., & Lie-Svendsen, Ø. 2011, Surveys in Geophysics, 32, 1
Elgarøy, E. Ø. 1977, Solar noise storms.
Forbes, T. G., Linker, J. A., Chen, J., et al. 2006, Space Sci. Rev., 123, 251
Forbush, S. E. 1946, Physical Review, 70, 771
Ganse, U., Kilian, P., Vainio, R., & Spanier, F. 2012, Sol. Phys., 280, 551
Garcia, H. A. 1994, Sol. Phys., 154, 275
Gary, D. E. & Hurford, G. J. 2004, in Astrophysics and Space Science Library, Vol. 314, Astrophysics and Space Science Library, ed. D. E. Gary & C. U. Keller, 71
Gopalswamy, N. 2006, Geophysical Monograph Series, 165, 207
Gopalswamy, N. 2011, in Planetary, Solar and Heliospheric Radio Emissions (PRE VII), ed. H. O. Rucker, W. S. Kurth, P. Louarn, & G. Fischer, 325–342
Gopalswamy, N., Akiyama, S., Mäkelä, P., Yashiro, S., & Cairns, I. H. 2016, arXiv e-prints, arXiv:1605.02223
Gopalswamy, N., Akiyama, S., Yashiro, S., & Mäkelä, P. 2010, in Astrophysics and Space Science Proceedings, Vol. 19, Magnetic Coupling between the Interior and Atmosphere of the Sun, 289–307
Gopalswamy, N., Mäkelä, P., & Yashiro, S. 2019, Sun and Geosphere, 14, 111
Gopalswamy, N., Yashiro, S., Michalek, G., et al. 2009, Earth Moon and Planets, 104, 295
Gosling, J., Skoug, R., & McComas, D. 2003, Geophysical research letters, 30
Gosling, J. T., Asbridge, J. R., Bame, S. J., et al. 1981, J. Geophys. Res., 86, 547
Grechnev, V. V., Lesovoi, S. V., Kochanov, A. A., et al. 2018, Journal of Atmospheric and Solar-Terrestrial Physics, 174, 46
Grechnev, V. V., Uralov, A. M., Kochanov, A. A., et al. 2016, Sol. Phys., 291, 1173
Habbal, S. R., Woo, R., Fineschi, S., et al. 1997, ApJ, 489, L103
Heras, A. M., Sanahuja, B., Lario, D., et al. 1995, ApJ, 445, 497
Hillaris, A., Bouratzis, C., & Nindos, A. 2016, Sol. Phys., 291, 2049
Hodgson, R. 1859, MNRAS, 20, 15
Hoeksema, J. T. 1984, PhD thesis, Stanford University, California
Howard, R. A., Michels, D. J., Sheeley, N. R., J., & Koomen, M. J. 1982, ApJ, 263, L101
Howard, R. A. & SECCHI Team. 2007, in American Astronomical Society Meeting Abstracts, Vol. 210, American Astronomical Society Meeting Abstracts #210, 28.12
Howard, R. A., Sheeley, N. R., J., Michels, D. J., & Koomen, M. J. 1985, J. Geophys. Res., 90, 8173
Hoyng, P., Duijveman, A., Machado, M. E., et al. 1981, ApJ, 246, L155
Hundhausen, A. J. 1972, Coronal Expansion and Solar Wind
Hundhausen, A. J. 1989, in Bulletin of the American Astronomical Society, Vol. 21, 856

Hundhausen, A. J. & Gosling, J. T. 1976, J. Geophys. Res., 81, 1436
Jebaraj, I. C., Magdalenić, J., Podladchikova, T., et al. 2020, A&A, 639, A56
Jian, L., Russell, C. T., Luhmann, J. G., & Skoug, R. M. 2006, Sol. Phys., 239, 393
Jian, L. K., Russell, C. T., Luhmann, J. G., Galvin, A. B., & Simunac, K. D. C. 2013, in American Institute of Physics Conference Series, Vol. 1539, Solar Wind 13, ed. G. P. Zank, J. Borovsky, R. Bruno, J. Cirtain, S. Cranmer, H. Elliott, J. Giacalone, W. Gonzalez, G. Li, E. Marsch, E. Moebius, N. Pogorelov, J. Spann, & O. Verkhoglyadova, 191–194
Jiang, C., Feng, X., Liu, R., et al. 2021, Nature Astronomy, 5, 1126
Kaiser, M. L., Kucera, T. A., Davila, J. M., et al. 2008, Space Sci. Rev., 136, 5
Kerdraon, A. & Delouis, J.-M. 1997, in Coronal Physics from Radio and Space Observations, ed. G. Trottet, Vol. 483, 192
Kilpua, E. K. J., Balogh, A., von Steiger, R., & Liu, Y. D. 2017, Space Sci. Rev., 212, 1271
Kim, R. S., Gopalswamy, N., Moon, Y. J., Cho, K. S., & Yashiro, S. 2012, ApJ, 746, 118
Kivelson, M. G. & Russell, C. T. 1995, Introduction to Space Physics
Klassen, A., Pohjolainen, S., & Klein, K. L. 2003, Sol. Phys., 218, 197
Klein, K.-L. 2021a, Frontiers in Astronomy and Space Sciences, 7, 105
Klein, K.-L. 2021b, Frontiers in Astronomy and Space Sciences, 7, 93
Klein, K. L. & Mouradian, Z. 2002, A&A, 381, 683
Kong, X. L., Chen, Y., Li, G., et al. 2012, ApJ, 750, 158
Koskinen, H. 2011, Physics of Space Storms: From the Solar Surface to the Earth (Germany: Springer-Verlag)
Krucker, S., Kontar, E. P., Christe, S., & Lin, R. P. 2007, ApJ, 663, L109
Krüger, A. 1984, Introduction to solar radio astronomy and radio physics.
Kumar, P., Innes, D. E., & Cho, K.-S. 2016, ApJ, 828, 28
Kumari, A., Ramesh, R., Kathiravan, C., & Gopalswamy, N. 2017, ApJ, 843, 10
Kundu, M. R. 1965, Solar radio astronomy
Kwon, R.-Y., Kramar, M., Wang, T., et al. 2013, ApJ, 776, 55
Kwon, R.-Y. & Vourlidas, A. 2018, Journal of Space Weather and Space Climate, 8, A08
Leblanc, Y., Dulk, G. A., & Bougeret, J.-L. 1998, Sol. Phys., 183, 165
Lemen, J. R., Title, A. M., Akin, D. J., et al. 2012, Sol. Phys., 275, 17
Lengyel-Frey, D. 1992, J. Geophys. Res., 97, 1609
Lepping, R. P., Wu, C. C., Berdichevsky, D. B., & Szabo, A. 2015, Sol. Phys., 290, 2265
Lin, R. P., Curtis, D. W., Larson, D. E., et al. 2008, Space Sci. Rev., 136, 241
Luhmann, J. G., Curtis, D. W., Schroeder, P., et al. 2008, Space Sci. Rev., 136, 117
Lyot. 1930, Bulletin Astronomique, 6, 305
MacQueen, R. M., Eddy, J. A., Gosling, J. T., et al. 1974, ApJ, 187, L85
Magdalenić, J., Marqué, C., Krupar, V., et al. 2014, ApJ, 791, 115
Magdalenić, J., Marqué, C., Zhukov, A. N., Vršnak, B., & Veronig, A. 2012, ApJ, 746, 152
Mäkelä, P., Gopalswamy, N., Akiyama, S., Xie, H., & Yashiro, S. 2011, Journal of Geophysical Research (Space Physics), 116, A08101
Mancuso, S., Frassati, F., Bemporad, A., & Barghini, D. 2019, A&A, 624, L2
Mann, G. 2015, Journal of Plasma Physics, 81, 475810601
Mann, G., Aurass, H., & Warmuth, A. 2006, A&A, 454, 969
Mann, G., Klassen, A., Classen, H. T., et al. 1996, A&AS, 119, 489
Mason, G. M., Korth, A., Walpole, P. H., et al. 2008, Space Sci. Rev., 136, 257
McCauley, P. I., Cairns, I. H., White, S. M., et al. 2019, Sol. Phys., 294, 106
McLean, D. J. & Labrum, N. R. 1985, Solar radiophysics : studies of emission from the sun at metre wavelengths
Melnik, V. N., Brazhenko, A. I., Konovalenko, A. A., et al. 2018, Sol. Phys., 293, 53
Melrose, D. B. 1980, Space Sci. Rev., 26, 3
Melrose, D. B. 2017, Reviews of Modern Plasma Physics, 1, 5
Mewaldt, R. A., Cohen, C. M. S., Cook, W. R., et al. 2008, Space Sci. Rev., 136, 285

Meyer, P., Parker, E. N., & Simpson, J. A. 1956, Physical Review, 104, 768
Morosan, D. E., Palmerio, E., Lynch, B. J., & Kilpua, E. K. J. 2020, A&A, 633, A141
Mugundhan, V., Ramesh, R., Kathiravan, C., Gireesh, G. V. S., & Hegde, A. 2018, Sol. Phys., 293, 41
Müller, D., Nicula, B., Felix, S., et al. 2017, A&A, 606, A10
Müller-Mellin, R., Böttcher, S., Falenski, J., et al. 2008, Space Sci. Rev., 136, 363
Nelson, G. J. & Melrose, D. B. 1985, in Solar Radiophysics: Studies of Emission from the Sun at Metre Wavelengths, ed. D. J. McLean & N. R. Labrum, 333–359
Ness, N. F. & Wilcox, J. M. 1964, Phys. Rev. Lett., 13, 461
Neugebauer, M., Forsyth, R. J., Galvin, A. B., et al. 1998, J. Geophys. Res., 103, 14587
Newkirk, Gordon, J. 1961, ApJ, 133, 983
Nindos, A. 2020, Frontiers in Astronomy and Space Sciences, 7, 57
Nindos, A., Alissandrakis, C. E., Hillaris, A., & Preka-Papadema, P. 2011, A&A, 531, A31
Nindos, A., Aurass, H., Klein, K. L., & Trottet, G. 2008, Sol. Phys., 253, 3
Oh, S. Y., Yi, Y., & Kim, Y. H. 2007, Sol. Phys., 245, 391
Oliveira, D. M. 2017, Brazilian Journal of Physics, 47, 81
Palmerio, E., Kilpua, E. K. J., Möstl, C., et al. 2018, Space Weather, 16, 442
Parks, G. K. 2004, Physics of space plasmas : an introduction
Payne-Scott, R., Yabsley, D. E., & Bolton, J. G. 1947, Nature, 160, 256
Pesnell, W. D., Thompson, B. J., & Chamberlin, P. C. 2012, Sol. Phys., 275, 3
Pick, M. & Vilmer, N. 2008, A&A Rev., 16, 1
Pohjolainen, S. & Lehtinen, N. J. 2006, A&A, 449, 359
Pohjolainen, S. & Sheshvan, N. T. 2018, in 2018 2nd URSI Atlantic Radio Science Meeting (AT-RASC), 1–3
Pohjolainen, S., van Driel-Gesztelyi, L., Culhane, J. L., Manoharan, P. K., & Elliott, H. A. 2007, Sol. Phys., 244, 167
Priest, E. 2014, Magnetohydrodynamics of the Sun
Rao, U. R., McCracken, K. G., & Bukata, R. P. 1967, J. Geophys. Res., 72, 4325
Reames, D. V. 1990, ApJS, 73, 235
Reames, D. V. 2004, Advances in Space Research, 34, 381
Reames, D. V. 2017, Solar Energetic Particles: A Modern Primer on Understanding Sources, Acceleration and Propagation, Vol. 932
Reid, H. A. S. 2020, Frontiers in Astronomy and Space Sciences, 7, 56
Reid, H. A. S. & Ratcliffe, H. 2014, Research in Astronomy and Astrophysics, 14, 773
Reiner, M. J., Kaiser, M. L., Fainberg, J., & Stone, R. G. 1998, J. Geophys. Res., 103, 29651
Reiner, M. J., Kaiser, M. L., Gopalswamy, N., et al. 2001, J. Geophys. Res., 106, 25279
Richardson, J. D., Liu, Y., Wang, C., & Burlaga, L. F. 2006, Advances in Space Research, 38, 528
Riley, P., Linker, J. A., Mikić, Z., et al. 2006, ApJ, 653, 1510
Robinson, P. A. & Cairns, I. H. 2000, Geophysical Monograph Series, 119, 37
Robinson, R. D. 1978, Australian Journal of Physics, 31, 533
Robinson, R. D. & Stewart, R. T. 1985, Sol. Phys., 97, 145
Russell, C. T. & Mulligan, T. 2002, Planet. Space Sci., 50, 527
Saito, K., Poland, A. I., & Munro, R. H. 1977, Sol. Phys., 55, 121
Sarris, E. T. & van Allen, J. A. 1974, J. Geophys. Res., 79, 4157
Sauvaud, J. A., Larson, D., Aoustin, C., et al. 2008, Space Sci. Rev., 136, 227
Schatten, K. H., Wilcox, J. M., & Ness, N. F. 1969, Sol. Phys., 6, 442
Scherrer, P. H., Schou, J., Bush, R. I., et al. 2012, Sol. Phys., 275, 207
Schwenn, R. 2006, Living Reviews in Solar Physics, 3, 2
Shanmugaraju, A., Moon, Y. J., Cho, K. S., et al. 2005, Sol. Phys., 232, 87
Shea, M. A. & Smart, D. F. 1990, Sol. Phys., 127, 297
Shen, C., Liao, C., Wang, Y., Ye, P., & Wang, S. 2013, Sol. Phys., 282, 543
Sonett, C. P., Colburn, D. S., Davis, L., Smith, E. J., & Coleman, P. J. 1964, Phys. Rev. Lett., 13, 153
Spicer, D. S., Benz, A. O., & Huba, J. D. 1982, A&A, 105, 221

Strachan, L., Suleiman, R., Panasyuk, A. V., Biesecker, D. A., & Kohl, J. L. 2002, ApJ, 571, 1008
Thomas, R. J., Starr, R., & Crannell, C. J. 1985, Sol. Phys., 95, 323
Thomson, N. R., Rodger, C. J., & Dowden, R. L. 2004, Geophysical research letters, 31
Tidman, D. A. 1967, J. Geophys. Res., 72, 1799
Tousey, R. 1973, in Space Research Conference, Vol. 2, 713–730
Tsurutani, B. T. & Lin, R. P. 1985, J. Geophys. Res., 90, 1
van Allen, J. A. & Krimigis, S. M. 1965, J. Geophys. Res., 70, 5737
Vernazza, J. E., Avrett, E. H., & Loeser, R. 1981, ApJS, 45, 635
Vilmer, N., Pick, M., Schwenn, R., Ballatore, P., & Villain, J. P. 2003, Annales Geophysicae, 21, 847
von Rosenvinge, T. T., Reames, D. V., Baker, R., et al. 2008, Space Sci. Rev., 136, 391
Vourlidas, A. 2004, in Astrophysics and Space Science Library, Vol. 314, Astrophysics and Space Science Library, ed. D. E. Gary & C. U. Keller, 223
Vourlidas, A., Carley, E. P., & Vilmer, N. 2020, Frontiers in Astronomy and Space Sciences, 7, 43
Vourlidas, A., Howard, R. A., Esfandiari, E., et al. 2010, ApJ, 722, 1522
Vourlidas, A., Lynch, B. J., Howard, R. A., & Li, Y. 2013, Sol. Phys., 284, 179
Vourlidas, A. & Webb, D. F. 2018, ApJ, 861, 103
Vourlidas, A., Wu, S. T., Wang, A. H., Subramanian, P., & Howard, R. A. 2003, ApJ, 598, 1392
Vršnak, B. & Cliver, E. W. 2008, Sol. Phys., 253, 215
Vršnak, B., Magdalenić, J., & Zlobec, P. 2004, A&A, 413, 753
Wang, L., Lin, R. P., Krucker, S., & Mason, G. M. 2012, ApJ, 759, 69
Wang, Y. M. & Sheeley, N. R., J. 1992, ApJ, 392, 310
Webb, D. F. & Howard, T. A. 2012, Living Reviews in Solar Physics, 9, 3
Weiss, A. A. 1963, Australian Journal of Physics, 16, 526
White, S. M. 2007, Asian Journal of Physics, 16, 189
White, S. M., Bastian, T. S., Bradley, R., Parashare, C., & Wye, L. 2005, in Astronomical Society of the Pacific Conference Series, Vol. 345, From Clark Lake to the Long Wavelength Array: Bill Erickson's Radio Science, ed. N. Kassim, M. Perez, W. Junor, & P. Henning, 176
Wild, J. P. & McCready, L. L. 1950, Australian Journal of Scientific Research A Physical Sciences, 3, 387
Wild, J. P., Murray, J. D., & Rowe, W. C. 1954, Australian Journal of Physics, 7, 439
Wild, J. P., Sheridan, K. V., & Neylan, A. A. 1959a, Australian Journal of Physics, 12, 369
Wild, J. P., Sheridan, K. V., & Trent, G. H. 1959b, in URSI Symp. 1: Paris Symposium on Radio Astronomy, ed. R. N. Bracewell, Vol. 9, 176
Wild, J. P., Smerd, S. F., & Weiss, A. A. 1963, ARA&A, 1, 291
Wilson, T. L., Rohlfs, K., & Hüttemeister, S. 2009, Tools of Radio Astronomy
Winglee, R. M. & Dulk, G. A. 1986, ApJ, 310, 432
Woods, T. N., Eparvier, F. G., Hock, R., et al. 2012, Sol. Phys., 275, 115
Wu, C. S., Wang, C. B., Yoon, P. H., Zheng, H. N., & Wang, S. 2002, ApJ, 575, 1094
Wu, C. S., Yoon, P. H., & Li, Y. 2000, ApJ, 540, 572
Yan, X., Xue, Z., Jiang, C., et al. 2022, Nature Communications, 13, 640
Yashiro, S., Gopalswamy, N., Michalek, G., et al. 2004, Journal of Geophysical Research (Space Physics), 109, A07105
Yurchyshyn, V., Yashiro, S., Abramenko, V., Wang, H., & Gopalswamy, N. 2005, ApJ, 619, 599

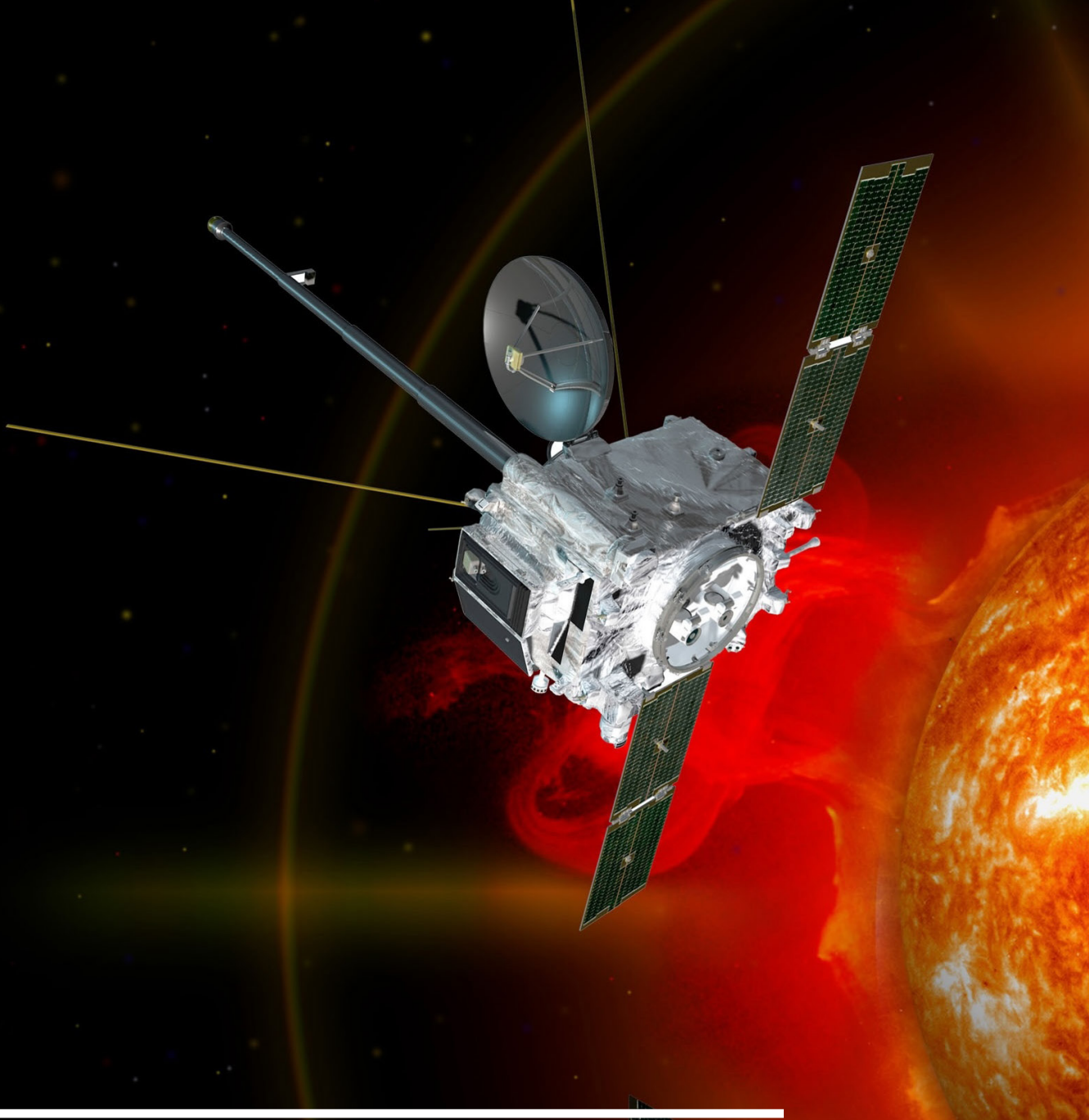

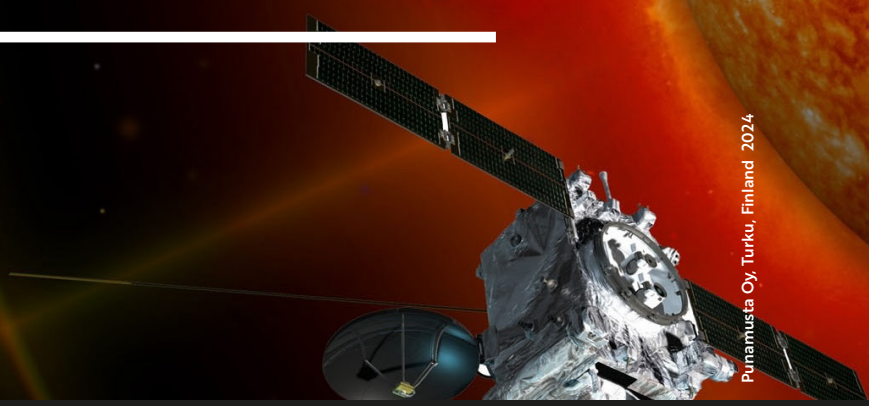

TURUN
YLIOPISTO
UNIVERSITY
OF TURKU

Painosalama Oy, Turku, Finland 2024

ISBN 978-951-29-9798-5 (print)
ISBN 978-951-29-9799-2 (pdf)
ISSN 0082-7002 (print)
ISSN 2343-3175 (online)